








# *Brugmansia suaveolens* leaf and flower-derived silver nanoparticle gel with antimicrobial, antioxidant, and anti-inflammatory potency

Firoj Tamboli<sup>1</sup> , Sameer Nadaf<sup>2\*</sup> , Sajid Mulani<sup>1</sup> ,  
Dinanath Gaikwad<sup>3</sup> , Harinath More<sup>4</sup> , Amir Tamboli<sup>2</sup> ,  
Shailendra Gurav<sup>5</sup> 

<sup>1</sup>Department of Pharmacognosy, Bharati Vidyapeeth College of Pharmacy, Kolhapur, Maharashtra, India.

<sup>2</sup>Bharati Vidyapeeth College of Pharmacy, Palus, Maharashtra, India.

<sup>3</sup>Department of Pharmaceutics, Bharati Vidyapeeth College of Pharmacy, Kolhapur, Maharashtra, India.

<sup>4</sup>Department of Pharmaceutical Chemistry, Bharati Vidyapeeth College of Pharmacy, Kolhapur, Maharashtra, India.

<sup>5</sup>Department of Pharmacognosy, Goa College of Pharmacy, Panaji, Goa, India.

\*Corresponding author: [sam.nadaf@rediffmail.com](mailto:sam.nadaf@rediffmail.com)

## Original Research

Received:

24 July 2024

Revised:

2 September 2024

Accepted:

10 September 2024

Published online:

10 January 2025

© 2025 The Author(s). Published by the OICC Press under the terms of the [Creative Commons Attribution License](#), which permits use, distribution and reproduction in any medium, provided the original work is properly cited.

## Abstract:

The rising demand for environmentally friendly technologies has spurred research into nanoparticle production methods utilizing biological agents. This study investigates the synthesis of silver nanoparticles (AgNPs) using extracts from *Brugmansia suaveolens* leaves and flowers as reducing agents. The nanoparticles were thoroughly characterized using DPPH assay, UV-visible spectroscopy, X-ray diffractometer (XRD), Fourier transform infrared spectroscopy (FTIR), and scanning electron microscopy (SEM). Both leaf and flower extracts were assessed for their antibacterial, antifungal, and anti-inflammatory properties, confirming the presence of bioactive compounds such as amines, carbohydrates, alkaloids, glycosides, saponins, and flavonoids. The synthesized AgNPs exhibited crystalline structures with average sizes of 102.7 nm (flower extract) and 75.2 nm (leaf extract), demonstrating robust antioxidant activities and effective inhibition against pathogens including *Staphylococcus aureus*, *Bacillus subtilis*, *Escherichia coli*, *Xanthomonas campestris*, and *Aspergillus niger*. These AgNPs were incorporated into gel formulations, evaluated for physical characteristics and *in vitro* diffusion properties. Notably, batch F6 showed exceptional skin penetration, with 84.96% of nanoparticles penetrating goat skin. Overall, these findings highlight the potential of AgNPs-loaded gel formulations as promising therapeutic options for chronic injuries and mild burns, warranting further *in vivo* studies to assess safety and efficacy.

**Keywords:** Angel's trumpet; Burns; Green synthesis; Metal nanoparticles; Wounds

## 1. Introduction

Nanotechnology exploits the unique properties of materials smaller than 100 nanometers (nm) to create innovative products with distinct characteristics not found in traditional macroscopic materials [1]. The substantial surface-area-to-volume ratio of nanomaterial is pivotal to their extensive use in biomaterials, electronics, nanotechnology, and the food industry [2].

Metal nanoparticles (NPs) have garnered significant attention due to their unique optical, chemical, photochemical, and electrical properties. Among them, silver nanoparticles

(AgNPs) stand out for their exceptional antibacterial properties, characterized by a broad spectrum and high surface area compared to other metallic nanoparticles [3]. This characteristic enables AgNPs to easily interact with microbial cells, enhancing their antibacterial effectiveness. Studies have demonstrated that even small amounts of AgNPs, such as 1 g, can confer antibacterial properties to hundreds of square meters of material [4]. AgNPs exhibit potent antimicrobial activity against over 650 different species of pathogenic microbes, making them a safe and effective organic antibacterial agent with a historical use spanning

millennia.

Silver is termed oligodynamic due to its ability to exert bactericidal effects even in minute quantities [1]. Silver nanoparticles (AgNPs) exhibit a broad spectrum of activities including antibacterial, antifungal, and antiviral properties, highlighting their versatility in combating various pathogens [5–8]. AgNPs exhibit a remarkable ability to permeate bacterial cell walls, disrupt cellular membrane integrity, and trigger cellular apoptosis [9]. Their antibacterial mechanism predominantly involves the release of Ag<sup>+</sup> ions, which inhibit bacterial growth by disrupting essential cellular processes such as respiratory enzymes, electron transport chains, and DNA replication [10]. AgNPs further disrupt bacterial replication by binding to sulfur-containing proteins, notably thiol groups (–SH), and DNA phosphates, leading to functional impairments in cellular machinery [11]. As a result, AgNPs are the most extensively studied and applied nanoparticles among all nano-sized metals due to their potent antimicrobial properties.

Metallic NPs can be synthesized using various chemical and physical methods [12, 13]. However, these conventional approaches are associated with drawbacks such as the use of hazardous solvents, generation of toxic byproducts, and high energy consumption [14]. To enhance the versatility of metallic nanoparticles and mitigate environmental impacts, there is a critical need to develop efficient, benign, and environmentally sustainable synthesis methods for NPs [15–17]. Green nanoscience represents a compelling field that has garnered considerable attention in contemporary discourse. Its primary aim is to foster the development of nanomaterials that are environmentally benign, safe for human exposure, and possess enduring economic viability [3, 18].

The development of different metallic NPs involving the use of plant-based materials, microbes [19], and biological wastes is referred to as a green synthesis approach [20]. A burgeoning area of nanoscience research involves the green synthesis of nanoparticles (NPs) utilizing abundant sources such as plants, marine organisms, and microorganisms [21, 22]. These methodologies offer numerous advantages over conventional physical and chemical processes, as they are cost-effective, environmentally sustainable, and easily scalable for large-scale production [21, 23]. Furthermore, green synthesis avoids the use of hazardous chemicals, high temperatures, pressures, or excessive energy inputs [21, 23]. Plant-mediated NP synthesis, in particular, has gained global prominence due to its accessibility, suitability for mass production, and generation of environmentally beneficial byproducts devoid of pathogenicity, unlike those produced by fungi and bacteria [24]. Numerous researchers have engaged in environmentally friendly methods to produce nanoscale AgNPs using diverse plant extracts. Examples include *Mangifera indica* leaf [25], *Murraya koenigii* leaf [22], *Piper cubeba* fruit [26], *Piper longum* L. [27], *Oxalis griffithii* [28], *Rumex nervosus* [29], *Oroxylum indicum* [30], *Pistacia atlantica* seeds [31], and *Psidium guajava* [32], among others.

*Brugmansia suaveolens* (Solanaceae), or angel's trumpet, is a versatile plant found globally across Asia, Australia,

Europe, and the Americas [33]. It typically grows as a 1–6-meter shrub or small tree [34]. Traditionally used for treating inflammation, wounds, ulcers, and skin infections, it has demonstrated antinociceptive [35], analgesic [36], antibacterial [37], and anticancer [38] properties in pharmacological studies. In traditional practices, inhalation of their leaf vapors has been used to alleviate respiratory ailments [33].

This botanical diversity underscores *Brugmansia suaveolens* as a promising candidate for exploring novel applications in green nanotechnology, particularly in the synthesis of AgNPs. Its rich phytochemical profile not only supports the reduction and stabilization of nanoparticles but also enhances their functional properties. By harnessing its medicinal attributes, such as antibacterial properties, researchers aim to develop innovative nanoparticle-based therapies. This approach not only expands the horizon of green nanotechnology but also holds promise for enhancing medical treatments. Furthermore, the use of *B. suaveolens* aligns with sustainable practices, minimizing environmental impact while promoting public health through eco-friendly and effective nanotechnology solutions.

Burn wound sepsis arises from compromised skin and systemic defenses, making burn patients vulnerable to microbial infections and high morbidity and mortality rates [39]. Traditional treatments like silver applications target these infections but often face issues such as neutralization by bodily fluids and potential toxicity to healing tissues [40]. In response to these challenges, our study introduces an environmentally benign approach using *Brugmansia suaveolens* leaf and flower extracts to synthesize AgNPs. It was hypothesized that developed AgNPs could potentially exhibit enhanced antibacterial, antioxidant, and anti-inflammatory properties compared to traditional silver treatments. This novel approach aimed to facilitate targeted delivery to burn wound sites via a gel formulation, ensuring sustained release and minimal systemic toxicity. It was anticipated that these biocompatible AgNPs would potentially accelerate wound healing processes, reduce microbial colonization, and mitigate the incidence of burn wound sepsis, thus offering a promising and sustainable therapeutic strategy for improving burn wound care.

## 2. Materials and methods

### 2.1 Collection of plant material

The flowers and leaves of *Brugmansia suaveolens* (Solanaceae) were sourced from the Satara region of Maharashtra, India, located at latitude 17°41'29" N and longitude 74°0'3.31" E. Initially, they were cleansed by washing with tap water followed by a rinse with double distilled water to eliminate any dust particles and foreign contaminants. The flowers were then dried in an oven at 40 °C for 2 days, while the leaves were dried in shade for 7 days separately. Subsequently, both flowers and leaves were pulverized using a blender or mixer, and the powdered materials were stored in separate glass containers until ready for use.

2.2 Preparation of extracts

To prepare the plant extracts 10 grams of each powdered plant material—flowers and leaves—were weighed and individually mixed with 100 mL of triple-distilled water. The mixtures were then heated in a water bath maintained at a temperature range of 60 – 70 °C for 30 minutes to ensure adequate extraction of bioactive compounds. This heating process facilitates the solubilization of phytochemicals from the plant material into the aqueous phase. After the heating period, the mixtures were allowed to cool to room temperature. Following cooling, the mixtures were filtered using a fine mesh or filter paper to remove large particulate matter. The filtered solutions were then subjected to centrifugation at 2000 rpm for 10 minutes. This centrifugation step helps to separate and remove any remaining dense biomaterials, such as cellular debris, that might affect the clarity and consistency of the extract. The resulting clear extract broth was collected and stored in a refrigerator at 4 °C to maintain stability until further use. The stored extracts were subsequently subjected to phytochemical screening. Alkaloids were tested using Dragendroff’s, Wagner’s, Hager’s, and Mayer’s tests to confirm their presence. Carbohydrates were assessed with Molisch’s and Fehling’s tests, while Benedict’s test was used to detect reducing sugars. Flavonoids were identified using Shinoda’s test, lead acetate solution, and NaOH test. The presence of saponins was confirmed through the foam test. Triterpenes were evaluated using the Liebermann-Burchard test, and glycosides, particularly anthraquinone glycosides, were tested accordingly. Steroids were examined using Salkowski, Liebermann-Burchard, and sulfur tests. Tannins were detected through 5% ferric chloride, 10% lead acetate, acetic acid, and potassium permanganate tests, and the presence of certain tannin types was further assessed using the dilute iodine test.

2.3 Synthesis of AgNPs

30 mL of a 0.1 M solution of AgNO<sub>3</sub> was placed in a flask, to which 15 mL of freshly prepared aqueous extract of *B. suaveolens* leaves was added with continuous stirring. The mixture was magnetically stirred at 30 – 35 °C for 20 minutes to initiate the formation of colloids. The reduction of Ag<sup>+</sup> ions to Ag<sup>0</sup> proceeded completely, evident from the noticeable dark-brown color of the reaction mixture. Following this, the colloidal solution containing AgNPs was centrifuged at 4000 rpm for 30 minutes. After cen-

trifugation, the AgNPs pellets were carefully collected and re-suspended in triple distilled water. This suspension was centrifuged again under the same conditions to ensure complete removal of any residual materials. This purification process was repeated twice to achieve thorough purification of the AgNPs. Finally, the purified AgNPs pellets were dried in an oven and stored for further characterization. The same procedure was repeated using an aqueous extract of *B. suaveolens* flowers [41].

2.4 Characterization of developed AgNPs

2.4.1 UV-vis spectroscopy studies

UV–vis spectrophotometry is a widely adopted and effective method for analyzing metal NPs [28]. In this study, the bioreduction process of AgNO<sub>3</sub> to synthesize AgNPs was monitored using a UV-Spectrophotometer (Double beam, Shimadzu, UV-800) operating in the wavelength range of 300 – 800 nm. This method allowed observing the characteristic wavelength and absorbance patterns associated with the formation of AgNPs, thereby confirming the successful reduction of AgNO<sub>3</sub>.

2.4.2 Scanning electron microscope (SEM) analysis

SEM is a powerful tool for characterizing nanoparticles due to its capability to provide high-resolution images of sample surfaces [42]. In this study, SEM was employed to investigate the surface morphology, size, and shape of the synthesized AgNPs. Prior to analysis, a small amount of the sample was coated with a thin layer of gold using a sputter coater and then mounted for SEM imaging using a scanning electron microscope. This approach facilitated detailed examination and characterization of the physical attributes of the AgNPs at the nanoscale level.

2.4.3 X-ray diffraction (XRD) analysis

X-ray diffraction (XRD) is the primary method for characterizing nanoparticles [43], particularly for identifying their crystalline structure. In this study, XRD analysis was conducted to determine the crystalline structure of the synthesized AgNPs using extracts from both leaves and flowers of *Brugmansia suaveolens*. The diffractograms were obtained using Cu K $\alpha$  radiation with a wavelength of 1.5406 Å over a 2 $\theta$  range of 30 – 90 °C. This technique allowed for precise identification and analysis of the crystallographic properties of the AgNPs, providing insights into their composition and structure at the atomic level [16, 44].

Table 1. Composition of gel formulations.

Ingredients	F1	F2	F3	F4	F5	F6	F7	F8	F9
Carbopol (gm)	1	1.5	2	-	-	-	-	-	-
Chitosan (gm)	-	-	-	1	1.5	2	-	-	-
Na-CMC (gm)	-	-	-	-	-	-	2	3	4
Glycerol (gm)	2	2	2	2	2	2	2	2	2
AgNPs (gm)	0.02	0.02	0.02	0.02	0.02	0.02	0.02	0.02	0.02
Glacial acetic acid (mL)	-	-	-	0.75	1.12	1.5	-	-	-
Triethanolamine	q.s.	q.s.	q.s.	-	-	-	-	-	-
Water (mL)	100	100	100	100	100	100	100	100	100

#### 2.4.4 FTIR Fourier transform infrared (FTIR) spectroscopy

FTIR spectroscopy was employed to identify the potential components in *Brugmansia suaveolens* that facilitate the biosynthesis of AgNPs [28]. The dried and powdered AgNPs were mixed with potassium bromide (KBr) to form pellets, and the FTIR spectrum was recorded using an FT-IR spectrophotometer (Shimadzu) within the range of 600 – 4000 cm<sup>-1</sup>. The obtained spectrum was analyzed by subtracting the pure KBr spectrum, allowing for the identification of functional groups and chemical bonds present in the AgNPs synthesized using extracts from *B. suaveolens* leaves and flowers [16, 44].

#### 2.4.5 Particle size analyzer

Most often, a crucial parameter of the AgNPs is their particle size distributions. Dynamic light scattering was undertaken to estimate the mean sizing and size distribution of AgNPs. Synthesized AgNPs were dispersed in distilled water, passed through a Millipore filter paper (0.22 µm), and processed for size estimation. Particle size estimation was performed thrice [29].

### 2.5 Pharmacological evaluation of AgNPs

#### 2.5.1 Antibacterial activity

The Agar well diffusion method is widely utilized to evaluate the antimicrobial activity of plant extracts or microbial products [45]. In this study, the antibacterial efficacy of freshly synthesized AgNPs against *Staphylococcus aureus*, *Bacillus subtilis*, *Escherichia coli*, and *Xanthomonas campestris* was assessed using the well diffusion technique. Overnight cultures of bacteria were adjusted to achieve approximately 10<sup>6</sup> colony-forming units (CFU) per milliliter. Agar plates inoculated with 100 µL of the bacterial suspensions were incubated for 1 hour at 37 °C. Wells of 5 mm diameter were then created in the agar, into which both AgNPs and a reference antibiotic (azithromycin) were added. The diameter of the clear zones of inhibition surrounding the wells was measured after overnight incubation of the plates [29, 46].

#### 2.5.2 Antifungal activity

To evaluate the antifungal activity, the AgNPs were tested against *Aspergillus niger* using the same Well Diffusion method. Sabouraud Dextrose Agar (SDA) plates were inoculated with *A. niger* spores, and wells were created using a sterile cork borer. Clotrimazole was used as a positive control. After incubation at appropriate conditions, the diameter of the inhibition zones around the wells was measured to determine the antifungal activity of the AgNPs.

#### 2.5.3 Antioxidant activity

Antioxidants are compounds capable of counteracting the detrimental effects of oxidative processes within animal tissues [38, 47]. To evaluate the antioxidant properties of silver nanoparticles AgNPs synthesized using extracts from *Brugmansia suaveolens* flowers and leaves, their ability to scavenge free radicals was assessed using the stable radical DPPH, with ascorbic acid as a reference. AgNPs were

added to 1 mL of freshly prepared DPPH solution (1 mL in methanol) at concentrations ranging from 10 to 40 µg/mL followed by thorough vortexing. The mixture was then incubated in the dark at room temperature for 30 minutes. Absorbance was measured at 517 nm using a UV-vis spectrophotometer (Shimadzu, UV-800). The free radical scavenging activity was calculated using the formula,

$$\% \text{ DPPH Radical Scavenging Activity} = \frac{A_c - A_s}{A_c} \times 100 \quad (1)$$

where 'Ac' stands for the absorbance of the control and 'As' stands for the absorbance of the sample. The IC<sub>50</sub> value, representing the concentration of antioxidant material required to reduce the initial concentration of DPPH by 50%, was also calculated using the formula.

#### 2.5.4 In vitro anti-inflammatory activity

Protein denaturation plays a significant role in inflammation; hence, plant extracts that prevent denaturation are often investigated for their anti-inflammatory efficacy. A 0.2% (w/v) solution of egg albumin was prepared in PBS (pH 6.4). To this stock solution (5 mL), 50 µL of AgNPs at various concentrations (100, 200, 300, 400, and 500 µg/mL) were separately added. The samples were then heated at 72 °C for 5 minutes followed by cooling. The absorbance of these solutions was measured at 660 nm [4].

### 2.6 Preparation of gel formulation

As we observed superior activity in AgNPs synthesized using *B. suaveolens* leaves extract compared to those synthesized using *B. suaveolens* flowers extract, we selected the former for the preparation of gel formulations. Different batches of gels were formulated using Carbopol-940 (1, 1.5, and 2 g), CMC (2, 3, and 4 g), and Chitosan (1, 1.5, and 2 g) as gelling agents.

To prepare the gel bases, specified quantities of Carbopol-940, CMC, and Chitosan were separately mixed in double distilled water and allowed to hydrate for 30 minutes. Subsequently, glycerol (2 g) and AgNPs (0.02 g) were dispersed into each gel base with continuous stirring using a homogenizer. The developed systems were further hydrated for 3 hours with slow stirring. Finally, the pH of each system was adjusted to 7.0 using triethanolamine and stirred gently until a gel state was achieved. The composition of gel formulations with different gelling agents is presented in the Table 1.

### 2.7 Physicochemical evaluations

#### 2.7.1 Physical appearance

The gel formulations that incorporated AgNPs synthesized using *B. suaveolens* leaves extract were carefully examined to assess several visual characteristics. These included observing the color of the gel, ensuring it was uniform throughout, checking its consistency to ensure it was smooth and without lumps, and inspecting for any signs of phase separation where different components of the gel might have separated into distinct layers or phases.

### 2.7.2 pH

The pH of the gel formulations was determined using a digital pH meter. For the gel formulations containing AgNPs synthesized with *B. suaveolens* leaves extract, pH measurement is critical as it helps ensure that the formulation is within the desired pH range for optimal stability, compatibility with skin pH, and effectiveness of the active ingredients.

### 2.7.3 Viscosity

Viscosity is crucial in topical formulations like gels to ensure proper spread ability, ease of application, and adherence to the skin surface, thereby influencing the overall user experience and efficacy of the product. The viscosity of the formulated gels was quantified using a Brookfield viscometer (Model DV-II+Pro) at a rotational speed of 100 rpm. This measurement is essential as it provides information about the flow behavior and consistency of the gel formulations.

### 2.7.4 Centrifugation test

Formulation stability was assessed using a centrifuge (Remi, India). Specifically, each sample gel (10 g) was centrifuged at 3000 rpm for 30 minutes at room temperature. This procedure helps evaluate the physical integrity and phase separation tendencies of the gel formulations under simulated stress conditions, providing insights into their robustness and suitability for practical use [48].

### 2.7.5 Spreadability

The spreading ability of the gel preparations was determined by measuring the spreading width of 1 g of gel between two flat glass surfaces (7.5 cm apart) under a defined force for 60 seconds. This measurement provides insights into how effectively the gel can spread upon application to the skin, influencing its bioavailability and potential effectiveness [49].

### 2.7.6 Extrudability

Standard collapsible metal tubes with caps were employed to fill and seal the gel compositions. Approximately 20 g of gel was filled into each sealed collapsible tube. The closed end of the tube was firmly pressed, and a clamp was applied to prevent leakage. Upon removing the cap, pressure was applied to extrude the gel until the force was released [50].

### 2.7.7 In vitro diffusion studies

All gel formulations underwent in vitro diffusion across goat skin membranes using Franz diffusion cells. Phosphate buffer (pH 7.5) served as the receptor medium. Goat skin samples were prepared by cutting suitable-sized sections,

followed by a 30-minute immersion in phosphate buffer before experimentation. Each Franz cell received 10 mL of receptor medium, with the flat flange of the cells sealed with a membrane and secured using a metal clamp. The donor compartment was attached, and an additional 2 mL of receptor medium was injected with a plunger. Across all cells, a total of 12 mL of receptor medium was employed. Heating was facilitated using a water circulation jacket, and magnetic mixing at 50 rpm was employed throughout the study, which lasted approximately 6 hours. Samples were collected at 30-minute intervals and analyzed at 455 nm using a UV-Vis spectrophotometer. Following each withdrawal, an equivalent volume of buffer was replenished in the receptor medium. The data obtained were plotted against time to generate release profiles [51].

### 2.7.8 Determination of antibacterial and antifungal activity

Subsequently, the chosen batch was evaluated for its antibacterial activity against strains such as *Staphylococcus aureus*, *Bacillus subtilis*, *Escherichia coli*, and *Xanthomonas campestris*, and antifungal activity against *Aspergillus niger* using the agar well diffusion technique. Standard antibiotics including azithromycin and clotrimazole were used as controls for antibacterial and antifungal activities, respectively. The diameters of the inhibition zones were measured to assess efficacy.

### 2.8 Statistical analysis

After conducting the experiments and collecting data, statistical analysis was performed using one-way ANOVA (Analysis of Variance). This statistical method was chosen to evaluate the differences between the various experimental groups in terms of their mean values. The results of the analysis are expressed as mean values accompanied by their respective standard deviations (mean  $\pm$  standard deviation). Significance level of  $P < 0.05$  was considered statistically significant.

## 3. Result and discussion

### 3.1 Phytochemical screening of extracts

Characteristics of *B. suaveolens* leaf and flower extracts, as presented in Table 2, revealed distinct differences in their color and yield, suggesting variations in their chemical compositions. The flower extracts, characterized by a higher yield and distinct color, suggest a richer concentration of bioactive compounds compared to the leaf extracts. These constituents contribute to the higher yield and characteristic color observed in flower extracts [52]. The color and

Table 2. Characteristics of *B. suaveolens* extracts.

Particulars	Flower	Leaves
Solvent	Aqueous	Aqueous
Color	Yellowish red	Reddish green
Nature	Semisolid	Semisolid
% yield (w/w)	19.4	17

yield differences between the leaf and flower extracts can be attributed to the types and concentrations of bioactive compounds present. Flower extracts typically contain a diverse array of bioactive substances, including flavonoids, alkaloids, and essential oils. These compounds are often associated with vibrant colors and higher yields. Flavonoids and alkaloids, known for their antioxidant and antimicrobial properties, contribute significantly to the pharmacological potential of the extracts [44]. The higher yield observed in the flower extracts aligns with their rich phytochemical profile, which can be beneficial for applications requiring high concentrations of bioactive agents.

In contrast, leaf extracts, while also rich in bioactive compounds, often contain different types and concentrations of these substances, which is reflected in their lower yield and greenish coloration. The green color is primarily due to the presence of chlorophyll and other related pigments, which are less prevalent in flower extracts. The differences in chemical composition between leaves and flowers are well-documented, with flowers generally providing a more concentrated source of certain phytochemicals due to their reproductive role and the accumulation of secondary metabolites.

The higher yield and distinct color of the flower extract underscore its potential as a concentrated source of bioactive compounds. This attribute is particularly advantageous for applications in fields such as nanotechnology. For instance, the synthesis of AgNPs often requires reducing agents to facilitate efficient nanoparticle production. Flower extracts, with their abundant reducing agents, can enhance the synthesis process, leading to more effective and controlled nanoparticle formation. The rich phytochemical content of flower extracts can also be harnessed for various other applications, including the development of pharmaceuticals

and functional foods.

The use of aqueous solvents for the extraction of *B. suaveolens* extracts aligns with principles of sustainable and green chemistry. Aqueous extraction methods are preferable due to their safety, reduced toxicity compared to organic solvents, and cost-effectiveness. These methods not only support environmental sustainability but also offer scalability for industrial applications. The ability to obtain high yields of bioactive compounds using aqueous solvents highlights the viability of flower extracts from *B. suaveolens* as valuable resources for both pharmaceutical and nanotechnology sectors.

Phytochemical screening corroborated the presence of amine, carbohydrates, alkaloids, phenolic complexes, anthraquinone glycosides, saponins, triterpenes, flavonoids, steroids, terpenoids, and tannins (Table 3).

The positive results for alkaloids, carbohydrates, flavonoids, saponins, glycosides, and tannins in both leaf and flower extracts indicate a rich phytochemical profile. Alkaloids were confirmed through Dragendroff's, Wagner's, Hager's, and Mayer's tests, which were all positive. This suggests the presence of alkaloid compounds known for their therapeutic properties, including analgesic and antibacterial effects. Carbohydrates were identified in both extracts using Molisch's and Fehling's tests, although Benedict's test was negative, suggesting the presence of certain types of carbohydrates but not reducing sugars. Flavonoids were consistently detected in both extracts through Shinoda's, lead acetate solution, and NaOH tests, indicating their potential antioxidant and anti-inflammatory properties. Saponins, identified by the foam test, were present in both extracts, known for their antimicrobial and anti-inflammatory activities.

Interestingly, the tests for triterpenes (Liebermann Burchard

Table 3. Composition of gel formulations.

Chemical constituents	Test	Leaves extract	Flowers extract
Alkaloids	Dragendroff's test	+	+
	Wagner's test	+	+
	Hager's test	+	+
	Mayer's test	+	+
Carbohydrates	Molisch's test	+	+
	Fehling's test	+	+
	Benedict's test	-	-
	Shinoda's test	+	+
Flavonoids	Lead acetate solution.	+	+
	NaOH test	+	+
	Foam test	+	+
Saponins	Liebermann Burchard test	-	-
Triterpines	Test for Anthraquinone Glycosides	+	+
Glycosides	Salkowaski test	-	-
Steroids	Liebermann Burchard test	-	-
	Sulfur test	-	-
Tannins	5% Ferric chloride test	+	+
	10% lead acetate	+	+
	Acetic acid	+	+
	Pot. Permanganate	+	+
	Dil. Iodine	-	-

test) and steroids (Salkowaski, Liebermann Burchard, and sulfur tests) were negative in both extracts. This absence suggests that these particular classes of compounds are either not present or are in concentrations too low to be detected by these standard tests.

Tannins were found in both extracts, as confirmed by the 5% ferric chloride, 10% lead acetate, acetic acid, and potassium permanganate tests. These compounds are known for their astringent properties and potential health benefits, including antioxidant and antimicrobial activities. The dilute iodine test was negative, indicating the absence of certain tannin types or iodine-reactive compounds.

The rich presence of alkaloids, flavonoids, saponins, and tannins in the flower extract, combined with its higher yield, makes it a particularly valuable source for bioactive compounds. These findings support the use of the flower extract in applications requiring high phytochemical content, such as the synthesis of AgNPs. The bioactive compounds can act as reducing and stabilizing agents in the green synthesis of AgNPs, enhancing their formation and biological activity.

### 3.2 Synthesis of AgNPs

*B. suaveolens* flowers and leaf extracts were employed for the synthesis of AgNPs. The reduction of  $\text{Ag}^+$  ions to  $\text{Ag}^0$  nanoparticles occurred when the plant extract of *B. suaveolens* was treated with  $\text{AgNO}_3$  solution in a 2:1 ratio. This reduction process was completed within 30 minutes, as evidenced by the distinct color change to darkish-brown, confirming the formation of AgNPs (Fig. 1).

The synthesis of AgNPs using extracts from *B. suaveolens* flowers (Fig. 1B) and leaves (Fig. 1Y) successfully achieved. When the plant extracts were treated with a silver nitrate ( $\text{AgNO}_3$ ) solution (Fig. 1A and Fig. 1X) in a 2:1 ratio, the  $\text{Ag}^+$  ions were effectively reduced to  $\text{Ag}^0$  nanoparticles. This reduction process was marked by a noticeable color change to dark brown (Fig. 1C and Fig. 1Z), indicating the formation of AgNPs. Remarkably, this transformation occurred within 30 minutes, underscoring the efficiency of the *B. suaveolens* extracts as reducing agents.

The rapid reduction of silver ions to nanoparticles within such a short timeframe highlights the potent reducing capabilities of the phytochemicals present in the *B. suaveolens* extracts. The color change to dark brown served as a visual confirmation of the reduction process, suggesting that compounds like alkaloids, flavonoids, and tannins, known for their electron-donating properties, could have been instrumental in this process [53]. These bioactive compounds

might have facilitated the conversion of  $\text{Ag}^+$  ions to elemental silver ( $\text{Ag}^0$ ), thereby forming stable nanoparticles.

The abundant presence of flavonoids and tannins in the *B. suaveolens* extracts is pivotal not only for reducing but also for stabilizing the AgNPs. These compounds function as effective capping agents, preventing the aggregation of nanoparticles and maintaining their uniform dispersion [54]. Additionally, the presence of saponins and alkaloids in the extracts further enhances the stability and uniformity of the synthesized nanoparticles.

### 3.3 Characterization of developed nanoparticles

Nanoparticles synthesized using *B. suaveolens* leaves and flowers were characterized using the following characterization methods.

#### 3.3.1 UV-vis spectroscopy studies

The utilization of UV-visible spectroscopy to monitor the synthesis of AgNPs is a direct and dependable analytical approach. Central to this method is the principle of surface plasmon resonance (SPR). SPR arises when the conducting electrons on the surface of a metal nanoparticle oscillate in resonance with certain wavelengths of incident light, resulting in a characteristic absorbance peak. This phenomenon is responsible for the unique color and absorbance properties observed in colloidal solutions of AgNPs. Typically, SPR manifests as absorbance peaks around 435 nm, confirming the conversion of silver nitrate into AgNPs [55].

In this study, the synthesized AgNPs from *B. suaveolens* flower and leaf extracts displayed single maximum absorbance peaks at 450 nm (Fig. 2a) and 455 nm (Fig. 2b), respectively. These peaks suggested the successful formation of AgNPs, aligning with the expected SPR range for AgNPs. The slight variation in the peak positions could be attributed to differences in the phytochemical composition of the flower and leaf extracts, which influenced the size and surface properties of the nanoparticles [56, 57]. The single absorbance peaks observed in both cases indicated that the nanoparticles were likely spherical. Spherical nanoparticles typically exhibit a single SPR band, whereas anisotropic particles (those with non-spherical shapes) would show multiple SPR bands in the UV-visible spectra [58].

The effective synthesis of AgNPs using *B. suaveolens* extracts underscores their potential as powerful reducing and stabilizing agents. The observed clear SPR peaks confirm the successful reduction of  $\text{Ag}^+$  ions to elemental silver ( $\text{Ag}^0$ ), a process facilitated by the bioactive compounds

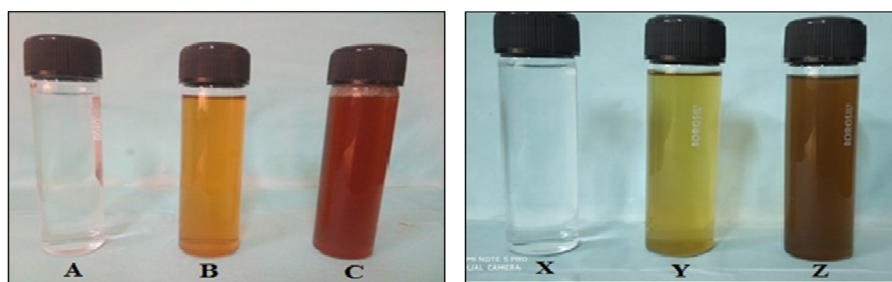


**Figure 1.** Formation of AgNPs. Tube A and X- silver nitrate, Tube B- Extract of *B. suaveolens* flowers, Tube C and Z- AgNPs colloidal solution, Tube Y- Extract of *B. suaveolens* leaf.

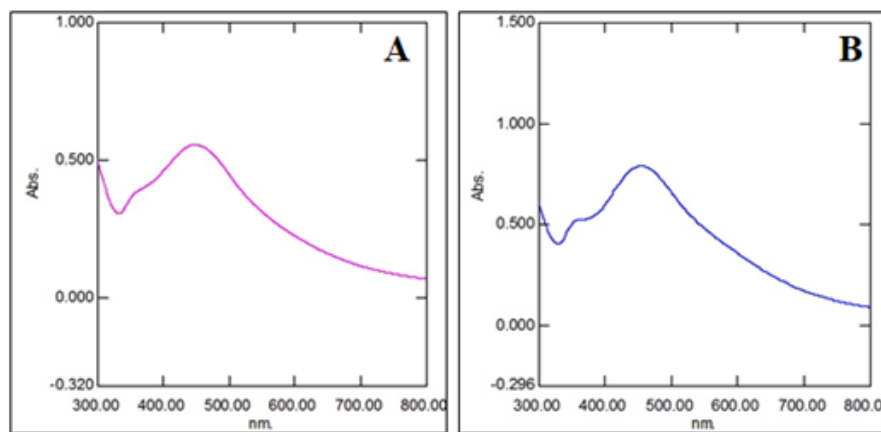


**Figure 2.** UV spectra of silver nanoparticle produced using (A) *B. suaveolens* flowers and (B) leaves extracts.

present in the extracts. Specifically, alkaloids, flavonoids, and tannins play a crucial role in this reduction process. These compounds contribute to the reduction of silver ions by donating electrons, which is essential for the formation of metallic nanoparticles. Flavonoids, with their polyphenolic structure, are particularly effective in reducing metal ions and stabilizing the nanoparticles due to their ability to form complex structures with the silver ions. Alkaloids and tannins also support this process by providing additional reducing power and stabilizing the nanoparticles, preventing their aggregation. The stabilization of AgNPs by these compounds not only enhances their formation but also ensures their stability in suspension.

### 3.3.2 Scanning electronic microscope (SEM)

SEM was employed to examine the morphology of synthesized metallic NPs. As seen in Fig. 3, AgNPs produced using *B. suaveolens* flowers extract (Fig. 3A and Fig. 3B) and leaves extract (Fig. 3C and Fig. 3D) displayed a granular appearance and appeared to be clustered together. This clustering might be attributed to the forces within the parti-

cles that lead to agglomeration [59].

The granular appearance observed in the SEM images suggests that the synthesized silver AgNPs exhibit a relatively uniform shape and size, indicating a consistent synthesis process. However, the presence of agglomeration in the images may be attributed to van der Waals forces or other intermolecular interactions commonly found in nanoparticle systems. These interactions can lead to the aggregation of individual nanoparticles, resulting in the clustered appearance observed.

Agglomeration of nanoparticles has significant implications for their various applications. While it can sometimes enhance specific properties, such as increased surface area for catalytic reactions, it can also negatively impact other characteristics, such as dispersion stability and reactivity. Therefore, optimizing nanoparticles for particular applications often requires the implementation of stabilization techniques to control agglomeration.

In this study, the observed agglomerates were loosely connected, which could be attributed to the unique properties of the *B. suaveolens* extracts used in the synthesis of AgNPs.

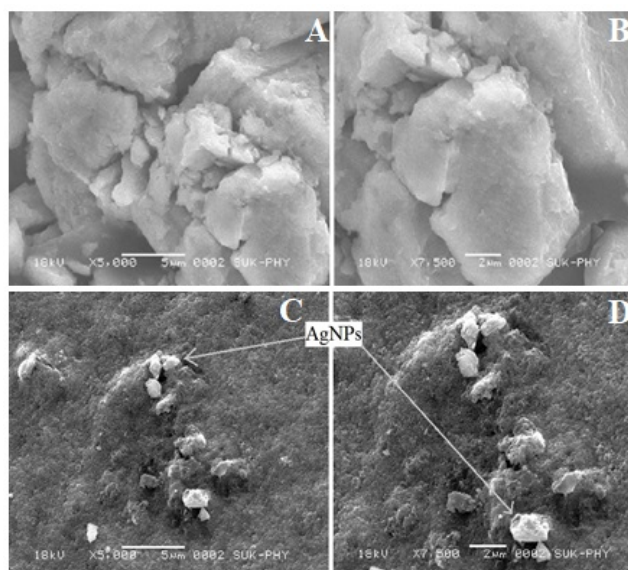


**Figure 3.** SEM images of AgNPs produced using (A and B) *B. suaveolens* flowers and (C and D) leaves extracts.

The phytochemicals present in these extracts not only facilitated the reduction of silver ions but also acted as effective capping agents. These compounds provide steric hindrance, which helps to prevent excessive agglomeration and promotes a more stable dispersion of the nanoparticles. The role of these phytochemicals in capping and stabilizing the nanoparticles underscores the advantages of using *B. suaveolens* extracts in green synthesis methods, contributing to the production of well-dispersed and stable NPs [60].

### 3.3.3 XRD

The XRD was employed for authenticating the crystallinity of their structure and nature of silver NPs prepared with the use of *B. suaveolens*.

The X-ray diffraction (XRD) analysis of biogenically created AgNPs using *B. suaveolens* flower extract was recorded within the  $2\theta$  range of  $30\text{--}90^\circ$ , as depicted in Fig. 4A. The XRD pattern illustrates the face-centered cubic (fcc) configuration of AgNPs, showing distinct diffraction peaks at  $37.23^\circ$  (111),  $44.23^\circ$  (200),  $64.59^\circ$  (220), and  $77.30^\circ$  (311). The diffraction peak at  $37.23^\circ$  exhibits a strong diffraction intensity, signifying the predominant orientation of the silver crystals along the (111) plane. The maximum peak intensity at the (111) plane, coupled with a narrow full width at half maximum (FWHM), suggests a high degree of crystallinity in the AgNPs synthesized using *B. suaveolens* flower extract [61].

The X-ray diffraction (XRD) analysis of biogenically created AgNPs using *B. suaveolens* flower extract was recorded within the  $2\theta$  range of  $30\text{--}90^\circ$ , as depicted in Fig. 4A. The X-ray diffraction (XRD) analysis of the synthesized AgNPs revealed a face-centered cubic (fcc) crystal structure, as evidenced by the distinct diffraction peaks observed at  $37.23^\circ$  (111),  $44.23^\circ$  (200),  $64.59^\circ$  (220), and  $77.30^\circ$  (311).

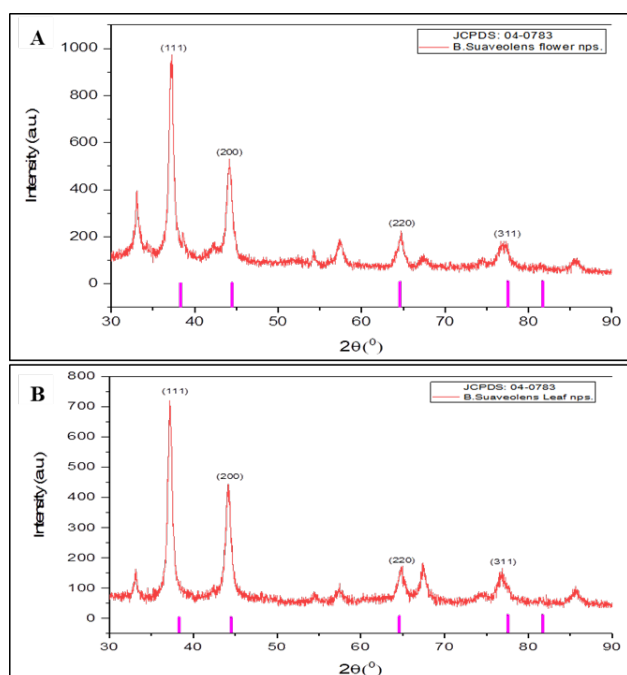


**Figure 4.** XRD spectra of AgNPs developed using (A) *B. suaveolens* flowers and (B) leaves extract.

The peak at  $37.23^\circ$  is particularly significant, corresponding to the (111) plane, which is often the most intense and indicative of the predominant orientation in fcc metals. This strong diffraction peak suggests that the silver nanoparticles exhibit a preferential growth direction along the (111) plane, which is a characteristic feature of high-quality crystalline materials.

The high intensity of the (111) peak, coupled with a narrow full width at half maximum (FWHM), indicates a high degree of crystallinity in the AgNPs. A narrow FWHM generally reflects fewer defects and a more uniform size distribution of the nanoparticles, which are key attributes for enhanced optical, catalytic, and electronic properties [54]. The observed fcc structure and prominent (111) peak align with the standard diffraction pattern for silver, confirming that the nanoparticles synthesized using *B. suaveolens* flower extract are indeed well-formed and crystalline.

This high crystallinity is advantageous for various applications of AgNPs, including in catalysis, where uniform particle size and well-defined crystal structure can lead to improved performance. The use of *B. suaveolens* flower extract in the synthesis process appears to facilitate the formation of well-structured nanoparticles, underscoring its efficacy as a green synthesis agent.

Similarly, the XRD configuration of AgNPs produced using *B. suaveolens* leaf extract, shown in Fig. 4B, also illustrated the face-centered cubic configuration. The diffraction peaks for the leaf extract-derived AgNPs were observed at  $37.12^\circ$  (111),  $44.14^\circ$  (200),  $64.89^\circ$  (220), and  $77.04^\circ$  (311). Notably, there are slight variations in the peak positions when compared to those of the AgNPs derived from the flower extract. The minor differences in peak positions and intensities could be attributed to variations in the phytochemical composition and concentration of the leaf extract compared to the flower extract. These variations may influence the particle size, shape, and overall crystallinity of the synthesized nanoparticles. For instance, differences in the types and amounts of reducing agents and stabilizers present in the leaf extract could affect the growth and stabilization of the nanoparticles, leading to subtle shifts in the XRD peaks. The observed differences in the XRD patterns highlight the influence of extract composition on the synthesis of AgNPs, emphasizing the role of specific phytochemicals in determining the structural properties of the nanoparticles [62]. The strong and sharp diffraction peak at the (111) plane in both flower and leaf extract-derived AgNPs indicated that the nanoparticles were predominantly oriented in this plane, a common characteristic of fcc AgNPs. Literature sources frequently reported similar diffraction peaks for AgNPs synthesized using various biological and chemical methods. For example, AgNPs synthesized using plant extracts like *Plantago lanceolata* [63] and *Gardenia resinifera* [64] also exhibited peaks near these positions and symmetry.

### 3.3.4 Particle size

The average particle sizes of AgNPs synthesized using *B. suaveolens* flowers and leaves were determined to be 102.7 nm (PDI 0.394) and 75.2 nm (PDI 0.127), respectively, as shown in Fig. 5. The particle size distribution indicates

that the AgNPs derived from flower extracts were relatively larger compared to those from leaf extracts. PDI values suggest that the nanoparticles from leaf extracts had a narrower size distribution and higher uniformity.

The larger average particle size of 102.7 nm for flower extract-derived AgNPs compared to the 75.2 nm for leaf extract-derived AgNPs might be attributed to the distinct phytochemical compositions of the extracts. The varied concentrations and types of flavonoids, alkaloids, and other phytochemicals present in the flower extract could alter the reduction kinetics and stabilization processes, resulting in larger particles. In contrast, the leaf extract, with its different phytochemical profile, may lead to a more controlled and uniform nucleation process, resulting in smaller and more uniformly sized NPs.

These findings underscore the importance of phytochemical composition in determining the characteristics of biogenically synthesized nanoparticles. The richer and potentially more complex mix of reducing agents and stabilizers in the flower extract likely promoted the formation of larger NPs, whereas the relatively simpler or different composition of the leaf extract resulted in smaller, more uniform particles. This variation in particle size and distribution has implications for the applications of these AgNPs, as different sizes can affect their antimicrobial properties, stability, and other functional attributes.

### 3.3.5 FTIR study

The FTIR spectra of AgNPs synthesized using *B. suaveolens* flower and leaf extracts are shown in Fig. 6. The spectrum of AgNPs derived from the flower extract (Fig. 6A) revealed characteristic peaks at 3007.97  $\text{cm}^{-1}$ , 2869.88  $\text{cm}^{-1}$ , and 1714.10  $\text{cm}^{-1}$ , corresponding to =C-H stretch, C-H stretch, and C=O stretch, respectively. These peaks indicate the presence of organic compounds such as aliphatic hydrocarbons and carbonyl groups, which likely functioned as reducing and capping agents during the synthesis of AgNPs. Additionally, peaks at 1344.45  $\text{cm}^{-1}$  and 947.85  $\text{cm}^{-1}$ , associated with C-N stretch and =C-H stretch, respectively, suggest the involvement of aromatic amines and alkenes in the nanoparticle formation process.

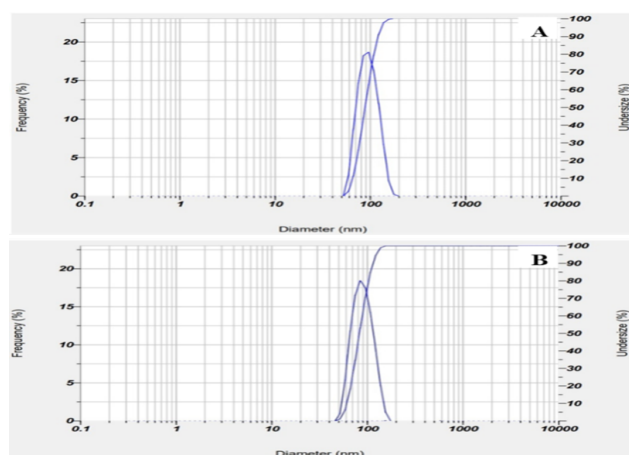


**Figure 5.** Particle size distribution of synthesized AgNPs using (A) *B. suaveolens* flowers and (B) leaves extracts.

Conversely, the FTIR spectrum of AgNPs synthesized from the leaf extract (Fig. 6B) exhibited distinct peaks, including =C-H stretch at 3088.98  $\text{cm}^{-1}$  and C=O stretch at 1747.86  $\text{cm}^{-1}$ , along with various bending modes indicative of aromatic compounds and alkynes. These peaks signify the presence of organic compounds that are instrumental in the synthesis of nanoparticles. Differences in peak intensities and the presence of additional peaks between the two spectra indicate variations in the phytochemical compositions of the flower and leaf extracts.

The differences in FTIR spectra underscore the impact of the specific phytochemical profiles of the plant extracts used in the green synthesis of AgNPs. The variation in organic compounds, such as aliphatic hydrocarbons, carbonyl groups, aromatic amines, and alkenes, highlights the importance of selecting appropriate plant materials and extraction methods to optimize the properties of biogenically synthesized NPs. These organic compounds not only facilitated the reduction of silver ions to form AgNPs but also played a critical role in stabilizing the nanoparticles and preventing their aggregation, thereby influencing their size, shape, and overall stability.

## 3.4 Pharmacological evaluation of developed AgNPs

### 3.4.1 Antibacterial activity

AgNPs synthesized from *B. suaveolens* flowers exhibited inhibition zones with diameters ranging from 10.2 mm to 15.19 mm against the tested bacterial strains. Detailed results are shown in Table 4 and Fig. 7. The largest inhibition zone was observed against *Xanthomonas campestris* (15 mm) (Fig. 7D), followed by *E. coli* (13 mm) (Fig. 7C), *B. subtilis* (12 mm) (Fig. 7B), and *S. aureus* (10 mm) (Fig. 7A). Azithromycin demonstrated significantly ( $P < 0.05$ ) larger zones of inhibition compared to AgNPs across all tested bacterial strains. This difference in efficacy could be attributed to variations in the concentration of bioactive compounds present in the flower extract, affecting the synthesis and potency of AgNPs against different bacterial species.

In contrast, AgNPs synthesized from *B. suaveolens* leaves

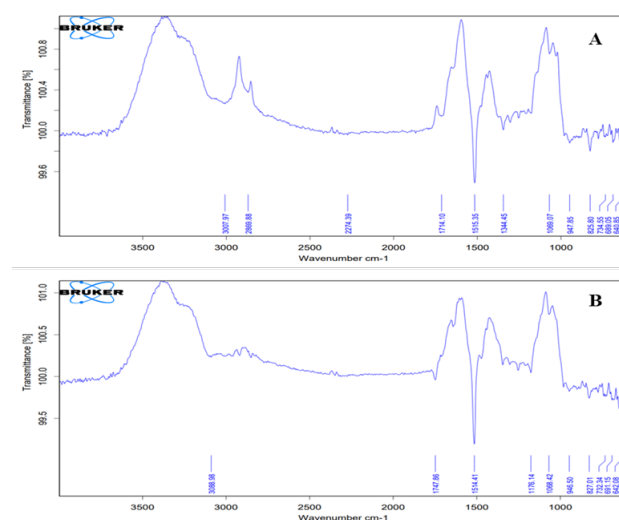


**Figure 6.** FTIR spectra of AgNPs produced using (A) *B. suaveolens* flowers and (B) leaves extracts.

**Table 4.** Zone of the inhibition of AgNPs against microorganisms.

Sample	Zone of inhibition diameter (mm)			
	<i>S. aureus</i>	<i>B. subtilis</i>	<i>E. coli</i>	<i>X. campestris</i>
<i>Flowers</i>				
AgNPs	10.2 ± 0.70	12.11 ± 0.87	13.17 ± 0.94	15.19 ± 1.37
Azithromycin (Std.)	15.20 ± 0.90	16.31 ± 0.52	18.22 ± 0.48	19.16 ± 0.83
<i>Leaves</i>				
AgNPs	11.13 ± 0.92	9.25 ± 0.25	13.14 ± 1.2	11.27 ± 0.82
Azithromycin (Std.)	15.02 ± 0.75	14.22 ± 1.07	18.31 ± 1.02	17.08 ± 0.94

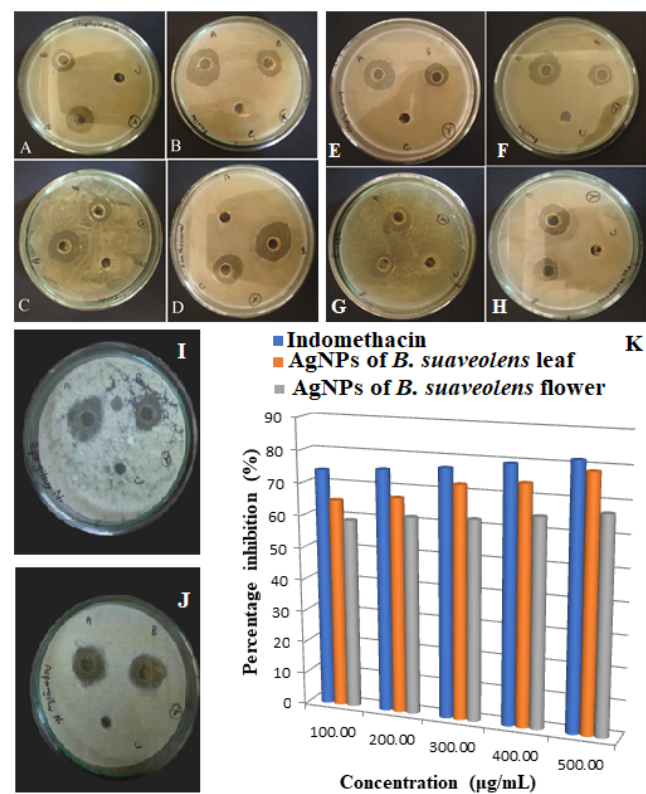


**Figure 7.** Comparative antibacterial and antifungal effects of standard antibiotics and AgNPs synthesized using *B. suaveolens* flowers and leaves extracts. (A-D) Antibacterial activity of AgNPs synthesized using *B. suaveolens* flowers against (A) *S. aureus*, (B) *B. subtilis*, (C) *E. coli*, and (D) *X. campestris*, compared to standard antibiotics. (E-H) Antibacterial activity of AgNPs synthesized using *B. suaveolens* leaves against (E) *S. aureus*, (F) *B. subtilis*, (G) *E. coli*, and (H) *X. campestris*, compared to standard antibiotics. Antifungal activity of AgNPs synthesized using (I) *B. suaveolens* leaves against *A. niger* and (J) *B. suaveolens* flowers compared to a standard antifungal. Each panel includes wells for AgNPs derived from flower or leaf extracts, a standard control (antibiotic or antifungal), and a negative control (no treatment). (K) Graphical representation of the *in-vitro* anti-inflammatory activity of AgNPs produced using *B. suaveolens* extracts and standard.

displayed inhibition zones ranging from 9.25 mm to 13.14 mm against the tested bacterial strains. Similar to the flower extract-derived AgNPs, the largest inhibition zone was observed against *E. coli* (13.14 mm) (Fig. 7H), followed by *Xanthomonas campestris* (11.27 mm) (Fig. 7G), *S. aureus* (11.13 mm) (Fig. 7E), and *B. subtilis* (9.25 mm) (Fig. 7F). Overall, Azithromycin exhibited significantly higher antibacterial activity against all tested bacterial strains compared to AgNPs, as evidenced by the larger zones of inhibition ( $P < 0.05$ ). Variations in the phytochemical composition of leaf extract may contribute to differences in the potency of AgNPs against different bacterial species. For comparison, the control samples, showed no zone of inhibition in both the flower and leaf extract groups, confirming that the observed antimicrobial effects are indeed

due to the AgNPs and not to any residual activity of the plant extracts themselves. It appears that the flower- and leaves-derived AgNPs demonstrated larger inhibition zones against gram-negative bacteria (*E. coli* and *X. campestris*) compared to gram-positive bacteria (*S. aureus* and *B. subtilis*). The variation in inhibition zones between gram-positive and gram-negative bacteria suggests differing susceptibility to synthesized AgNPs. Gram-negative bacteria, with their thinner cell walls, may be more susceptible to AgNPs' antimicrobial effects, resulting in larger inhibition zones. Conversely, the thicker cell walls of gram-positive bacteria may impede AgNPs' penetration, leading to smaller inhibition zones. This highlights the importance of considering bacterial cell wall structure when evaluating the efficacy of AgNPs as antimicrobial agents.

The observed trend, where gram-negative bacteria exhibit larger inhibition zones compared to gram-positive bacteria when exposed to AgNPs, aligns with findings reported in the literature [65, 66].

The antibacterial efficacy of AgNPs relies on several mechanisms, each potentially contributing to their ability to combat microbial pathogens. One significant mechanism could involve the release of silver ions ( $\text{Ag}^+$ ), hypothesized to bind to nucleic acids, potentially disrupting DNA replication and cellular processes. It is posited that  $\text{Ag}^+$  ions might adhere to bacterial cell walls and cytoplasm, potentially enhancing membrane permeability and disrupting cellular functions. AgNPs could have interacted directly with microbial cells, causing potential membrane denaturation, organelle rupture, and cell lysis due to their nanoscale size, potentially enabling penetration through bacterial cell walls. Additionally, it could be possible that AgNPs might have interfered with microbial signal transduction pathways, potentially inducing cell apoptosis and inhibiting cell proliferation. Another aspect that could be considered is the potential alteration of protein structures by  $\text{Ag}^+$  ions, hypothesized to interact with protein clusters or glycoproteins of pathogens, potentially leading to disruptions in cellular functions. Moreover, it is plausible that AgNPs might have generated reactive oxygen species (ROS), potentially further contributing to cellular membrane disruption, DNA alteration, and protein denaturation. Additionally, the deactivation of respiratory enzymes by  $\text{Ag}^+$  ions could have inhibited adenosine triphosphate (ATP) release, crucial for bacterial survival. These possibilities collectively underscore the diverse potential ways AgNPs could have combated bacterial growth [67].

However, the slightly lower efficacy of AgNPs compared to the standard antibiotic may be attributed to several factors. Firstly, the concentration of active compounds in the AgNPs could influence their antimicrobial effectiveness. The bioactive phytochemicals in the *B. suaveolens* extracts, while contributing to the reduction and stabilization of the nanoparticles, might be present in concentrations that are less potent than the standard antibiotic.

Secondly, the size and distribution of the nanoparticles play a crucial role in their antimicrobial activity. Smaller NPs generally have a larger surface area-to-volume ratio, which enhances their interaction with bacterial cells and improves their antimicrobial effectiveness. The observed particle sizes of AgNPs, being relatively larger than those of some commercially available NPs, could result in reduced efficacy due to lower surface reactivity and less effective penetration into bacterial cells.

Additionally, the specific mechanisms of action of AgNPs and the standard antibiotic differ. AgNPs exert their antimicrobial effects through various mechanisms, including the generation of ROS, disruption of bacterial cell membranes, and interaction with cellular components. The efficacy of AgNPs can vary depending on the bacterial strain and its resistance mechanisms. In contrast, standard antibiotics typically target specific bacterial processes or structures, and their effectiveness is well-documented against a broad spectrum of bacterial strains.

### 3.4.2 Antifungal activity

The AgNPs produced using flower extracts exhibited a zone of inhibition of  $17.2 \pm 0.97$  mm, which was significantly lower than the inhibition zone of  $21.11 \pm 0.34$  mm observed with the standard ( $P < 0.05$ ). Similarly, the AgNPs synthesized using leaf extracts showed a zone of inhibition of  $14.03 \pm 0.64$  mm, which was also significantly lower than the  $15.10 \pm 0.53$  mm inhibition zone of the standard ( $P < 0.05$ ). These results indicate that while AgNPs do possess antibacterial properties, their effectiveness is statistically lower than that of the standard reference, both for flower and leaf extract-based formulations (Fig. 7I and 7J). This corroborated the moderate antifungal activity of developed AgNPs. The results reveal that the zone of inhibitions produced by AgNPs derived from both flower and leaf extracts were notably lower compared to the standard antifungal agent. This suggests that while the synthesized AgNPs exhibited antifungal activity, their efficacy was moderate in comparison. Several factors may contribute to this outcome.

Firstly, the composition and concentration of bioactive compounds present in the plant extracts used for AgNP synthesis may have differed from those in the standard antifungal agent. Variations in phytochemical profiles could lead to differences in the potency of the synthesized AgNPs against fungal pathogens.

Additionally, the size and morphology of the AgNPs synthesized from flower and leaf extracts could influence their antifungal activity. It is plausible that AgNPs of different sizes and shapes exhibit varying degrees of efficacy against fungal pathogens.

Moreover, the method of synthesis and the presence of capping agents in the AgNP formulations may impact their antifungal activity. Green synthesis methods using plant extracts often result in the formation of AgNPs coated with biomolecules from the plant extracts. The nature and concentration of these biomolecules could affect the stability and bioactivity of the AgNPs against fungi.

### 3.4.3 *In vitro* anti-inflammatory activity

#### *Inhibition of albumin denaturation*

The investigation evaluated the inhibition of egg albumin denaturation by silver nanoparticles (AgNPs) synthesized using *B. suaveolens* leaf and flower extracts at varying concentrations. Results demonstrated a concentration-dependent inhibition of egg albumin denaturation by both types of AgNPs. Specifically, AgNPs synthesized from leaf extract exhibited inhibition percentages ranging from 65.04% to 78.67% across concentrations of 100 to 500  $\mu\text{g/mL}$ , while AgNPs synthesized from flower extract showed inhibition percentages ranging from 59.12% to 66.93% over the same concentration range. In comparison, the standard indomethacin displayed inhibition percentages ranging from 74.03% to 81.66% across the same concentration range. A graphical representation of the results is shown in Fig. 7K. ANOVA analysis indicates that there are significant differences in the inhibition percentages across different concentrations for both AgNPs and the standard. Based on the ANOVA results indicating significant differences

among concentration groups for both AgNPs synthesized from leaf and flower extracts, as well as for the standard (indomethacin), post-hoc Tukey tests were applied to determine specific concentration pairs that differed significantly from each other. For AgNPs synthesized from leaf and flower extracts, significant differences were found between the 100 µg/mL concentration and both the 400 µg/mL and 500 µg/mL concentrations ( $P < 0.05$ ). However, no significant differences were observed between the other concentration pairs, indicating that their inhibition percentages were not significantly different from each other.

For the standard (indomethacin), significant differences were identified between all concentration pairs ( $P < 0.05$ ), suggesting significant differences in inhibition percentages across all concentration levels. The one-way ANOVA comparing the inhibition percentages of egg albumin denaturation between the AgNPs synthesized from leaf extract, AgNPs synthesized from flower extract, and the standard (indomethacin) yielded a statistically significant difference among the groups ( $P < 0.05$ ). This indicates that there are significant variations in the inhibition percentages across the three groups, suggesting that the different treatments (AgNPs synthesized from leaf extract, AgNPs synthesized from flower extract, and indomethacin) have distinct effects on egg albumin denaturation.

The concentration-dependent inhibition of egg albumin denaturation by AgNPs suggests their potential as anti-inflammatory agents. Higher concentrations led to greater inhibition, indicating a dose-response relationship. Variations between leaf and flower extracts hint at differing bioactive constituents or synthesis methods. Despite slightly lower efficacy compared to indomethacin, AgNPs still demonstrated significant anti-inflammatory activity, offering a promising alternative to synthetic drugs. The anti-inflammatory activity of AgNPs could be linked to their ability to inhibit key inflammatory mediators and pathways. AgNPs might reduce the expression of pro-inflammatory cytokines such as TNF- $\alpha$ , IL-1 $\beta$ , and IL-6, which are pivotal in propagating inflammation. By down regulating these cytokines, AgNPs can help in reducing the inflammatory response [68].

#### 3.4.4 Antioxidant activity of synthesized AgNPs

The operation of wound repair is hampered significantly by a high level of oxidative damage within the area of injury [69]. Abundant ROS (reactive oxygen species) in the injured area can not only cause significant inflammatory reactions, making wounds susceptible but also impede the activities of innate stem cells and macrophages, preventing wound healing. On top of that, it is widely understood that ROS can inhibit angiogenesis and cause dysfunction in endothelial cells. In addition to the ROS produced by the wound, ROS produced by infectious bacteria can cause severe destruction of blood vessels and endothelial cells, leading to persistent wound development [70]. Therefore, testing of antioxidant potential of developed AgNPs is of great significance in topical applications. AgNPs synthesized using *B. suaveolens* flowers and leaves were examined for antioxidant activity using the DPPH method against

ascorbic acid which showed an IC<sub>50</sub> value of 3.39 µg/mL. Graphical representation is shown in Fig. 8D.

A one-way ANOVA was conducted to compare the effect of different concentrations of AgNPs on % inhibition of DPPH radical between flower-mediated and leaf-mediated extracts. The results showed no statistically significant difference, ( $P < 0.05$ ). A Tukey's HSD post hoc test confirmed the absence of significant differences across all concentrations. Leaf-mediated AgNPs consistently showed higher % inhibition compared to flower-mediated AgNPs, suggesting better antioxidant activity, although the difference was not statistically significant. This trend might be due to variations in the phytochemical composition of the extracts used for AgNP synthesis, affecting the antioxidant properties of the nanoparticles.

The significant antioxidant activity of these AgNPs may be attributed to the presence of bioactive compounds in the *B. suaveolens* extracts, which likely contribute to the reduction of ROS levels at the wound site. This reduction in oxidative stress could enhance the healing process by minimizing inflammatory responses and supporting the function of innate immune cells and endothelial cells. Moreover, the antioxidant properties of these AgNPs might also protect against the oxidative damage induced by bacterial infections, promoting more effective wound repair.

### 3.5 Formulation of gel incorporated with synthesized AgNPs

Based on the above results, it is clear that AgNPs synthesized using *B. suaveolens* leaf extract demonstrated superior activities. Consequently, we utilized these AgNPs for the formulation of a gel. AgNPs-loaded gels were successfully prepared using different concentrations of Carbopol 940, Na-CMA, and chitosan. This approach leverages the enhanced properties of leaf-mediated AgNPs to potentially create an effective topical application for wound healing and anti-inflammatory purposes.

#### 3.5.1 Evaluation of gel formulation

The preparation and characterization of AgNPs-loaded gels using different concentrations of Carbopol 940, Na-CMA, and chitosan revealed several notable findings. Visual inspection is an essential preliminary step in evaluating the quality and stability of gel formulations. It allows researchers to quickly assess whether the formulation has been properly prepared, whether the active ingredients are uniformly dispersed, and whether there are any visible defects or inconsistencies that could affect its effectiveness or usability. The gels exhibited slight variations in color, with Carbopol (Fig. 8A) and CMC-based gels (Fig. 8C) appearing slightly greenish-white, while chitosan-based gels were light brown (Fig. 8B). The All formulations maintained a pH range of 5.8 – 6.9, suitable for topical applications as it aligns with the natural pH of the skin, reducing the risk of irritation. In terms of viscosity, formulations with higher concentrations of Carbopol (F3), chitosan (F6), and Na-CMC demonstrated viscosities comparable to a marketed formulation. This is crucial as appropriate viscosity ensures the gel stays on the application site, providing sustained release of the active ingredient. Higher viscosity formulations

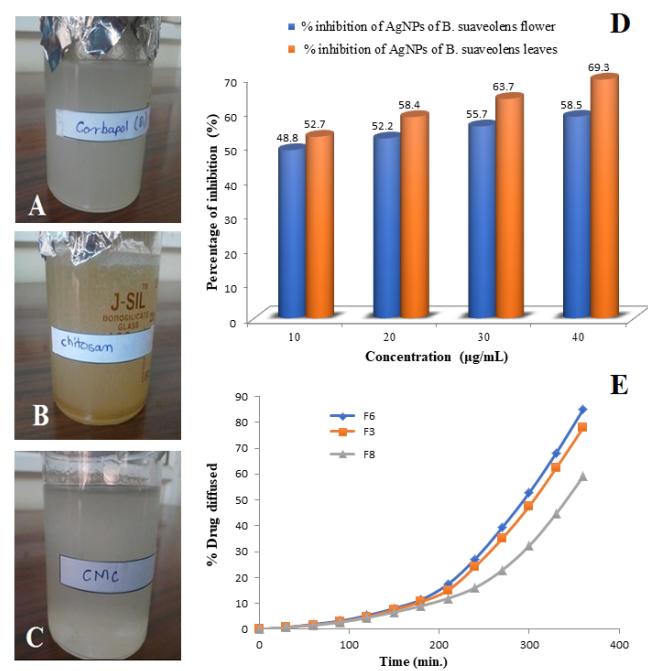


**Figure 8.** Formulated gels (A) Carbopol gel (B) Chitosan gel and (C) CMC-based gel. (D) Graphical illustration of antioxidant activity of synthesized AgNPs using *B. suaveolens* with IC<sub>50</sub> values of 22.63 and 19.75 µg/mL, synthesized AgNPs using *B. suaveolens* flowers and leaves, respectively, exhibited significant antioxidant activity. (E) *In vitro* diffusion profile of formulated gels.

(F3, F6, F9) also showed lower spreadability. Spreadability, which affects the bioavailability of the loaded components, was higher in the developed formulations compared to the marketed product, likely due to their lower viscosities. This implies that the developed gels can be applied more evenly over the skin, potentially enhancing the effectiveness of the active ingredients. The results of viscosities and spreadability are depicted in Table 5. Higher viscosity formulations (F3, F6, F9) showing lower spreadability and comparable viscosities to a marketed formulation is consistent with the idea that higher viscosity gels tend to stay at the application site longer, promoting sustained release of active ingredients. Additionally, the observation that the developed gels have higher spreadability than the marketed product suggesting and have lower viscosity formulations spread more easily over the skin, potentially improving the distribution of active ingredients. Extrudability, a measure of how easily the gel can be dis-

pensed from a tube, varied across formulations, with values ranging from 77.97 (F9) to 87.34 (F6). High extrudability is desirable as it indicates ease of use, ensuring that the gel can be applied without excessive force, which is important for patient compliance. The extrudability results are also detailed in Table 5. Finally, all formulations demonstrated stability under centrifugation tests, indicating that they can maintain their consistency and effectiveness under various conditions. This stability is essential for ensuring that the gels remain effective throughout their shelf life and during actual use. Comparing batches F1 to F9 with the commercial product revealed notable differences in pH, viscosity, spreadability, and extrudability, highlighting distinct characteristics between the formulated gels and the commercial product. Firstly, the pH of the commercial product ( $7.1 \pm 0.2$ ) was observed to be higher compared to most of the formulated batches (ranging from 5.8 to 6.9), indicating a more alkaline

**Table 5.** pH, Viscosity and Spreadability of gel formulations (mean S.D., n=3).

Batches	pH	Viscosity (cp)	Spreadability (mm)	Extrudability (%)	Appearance*
F1	5.8 ± 0.2	2406	46	81.42	++
F2	6.3 ± 0.2	2568	38	85.08	++
F3	6.6 ± 0.2	2890	35	87.00	++
F4	6.8 ± 0.2	2682	41	85.96	++
F5	6.7 ± 0.2	2867	38	84.57	++
F6	6.9 ± 0.2	3025	36	87.34	++
F7	6.1 ± 0.2	2484	48	81.70	++
F8	6.5 ± 0.2	2988	39	83.14	++
F9	6.6 ± 0.2	3103	37	77.97	+
Commercial product	7.1± 0.2	3037	34	91.47	+++

\* + fair, ++ good, +++ excellent

environment in the commercial product. This disparity may influence factors such as skin compatibility and stability, as pH can impact the efficacy and sensory experience of topical applications.

In terms of viscosity, the commercial product (3037 cp) fell within the range of viscosity values observed across batches F1 to F9 (ranging from 2406 to 3103 cp), indicating similar thickness or flow properties among the formulations. However, specific variations in the rheological behavior of each batch could still exist, potentially influencing factors such as application spreadability and retention on the skin. These variations might affect the user experience and the efficacy of the gel, as differences in viscosity can impact how easily the gel can be applied and how well it stays in place.

Spreadability measurements revealed slight differences between the commercial product (34 mm) and the formulated batches (ranging from 35 to 48 mm). While both demonstrated adequate spreadability for topical application, variations may influence user experience and the uniformity of product distribution across the skin surface.

Extrudability results showed that the commercial product (91.47%) exhibited higher ease of dispensation compared to most formulated batches, which ranged from 77.97% to 87.34%. This suggests that the commercial product may offer greater convenience in application, potentially enhancing user compliance and satisfaction. The superior extrudability of the commercial product indicates that it requires less force to dispense, making it easier for users to apply the desired amount of gel.

ANOVA results indicate significant differences between batches F1 to F9 and the commercial product in pH ( $P < 0.05$ ), viscosity ( $P < 0.05$ ), spreadability ( $P < 0.05$ ), and extrudability ( $P < 0.05$ ). These findings highlight distinct characteristics between the formulated gels and the commercial product; underscore the importance of careful formulation design and optimization to meet specific product requirements and user preferences.

### 3.5.2 Optimization of batch

Following the comprehensive assessment of all prepared batches, including pH, viscosity, spreadability, and extrudability, batches F3, F6, and F8 exhibited the most favorable outcomes. Consequently, these three batches were selected for further *in vitro* diffusion studies. Their promising initial performance suggested potential effectiveness and suitability for the intended application.

### 3.5.3 *In vitro* diffusion studies

The *in-vitro* diffusion study results for batches F3, F6, and F8, as illustrated in Fig. 8E, revealed distinct patterns of drug permeation across goat skin over a 6-hour period. Following the 6 h evaluation, Batch F6 exhibited the highest drug permeation percentage at  $84.96 \pm 4.18\%$ , followed by Batch F3 at  $77.92 \pm 3.67\%$ , and Batch F8 at  $59.06 \pm 3.99\%$ . Statistical analysis indicated significant differences ( $P < 0.05$ ) in drug permeation among the three batches, with Batch F6 demonstrating significantly higher permeation compared to both F3 and F8.

The observed differences in drug permeation across goat

skin among batches F3, F6, and F8, as determined by the *in vitro* diffusion study, are consistent with the specific compositions and optimization of these formulations.

Batch F6, which demonstrated the highest drug permeation, contained a higher concentration of chitosan (2 g) compared to batches F3 and F8. Chitosan is recognized for its mucoadhesive properties and capacity to enhance drug permeation across biological barriers. In this instance, the elevated chitosan concentration likely promoted stronger adhesion to the skin and facilitated enhanced drug diffusion, contributing to the notable increase in drug permeation observed in Batch F6. Conversely, Batch F8, which contained a higher concentration of Na-CMC (3 g), exhibited relatively lower drug permeation ( $59.06 \pm 3.99\%$ ) compared to batches F3 and F6. Na-CMC, primarily used as a viscosity modifier, lacks the mucoadhesive properties of chitosan. The increased viscosity from Na-CMC may have hindered drug diffusion across the skin barrier, resulting in the reduced drug permeation observed in Batch F8. The higher viscosity could create a thicker, more resistant layer, which impedes the movement of drug molecules through the skin. Batch F3, containing 2 g of Carbopol have been demonstrated intermediate drug permeation compared to batches F6 and F8. Carbopol is known for its role in increasing gel viscosity, which can enhance the stability of the formulation. However, its mucoadhesive properties are generally less pronounced than those of chitosan. The intermediate permeation observed in Batch F3 suggests that while Carbopol contributes to the formulation's viscosity and stability, it does not provide the same level of skin adhesion and permeability enhancement as chitosan. This indicates that Batch F3's performance in drug permeation is moderated by Carbopol's weaker mucoadhesive properties, resulting in drug permeation levels between those of the more effective chitosan-based Batch F6 and the less effective Na-CMC-based Batch F8.

### 3.5.4 Determination of antibacterial and antifungal activity

As we found batch F6 shows higher permeation across the goat skin membrane, only the F6 batch was selected for antibacterial and antifungal activities. Well diffusion assay was carried out for evaluating the antibacterial and antifungal efficacies of AgNPs-loaded gel against *Staphylococcus aureus*, *Bacillus subtilis*, *Escherichia coli*, and *Xanthomonas campestris* and *Aspergillus niger*. Results for well diffusion assay are shown in Fig. 9, which represents a zone of inhibitions for standard, extract, and control. For this study, antibacterial and antifungal activity was tested against standard commercial product and KANSEL-DS gel, respectively. Zones of inhibition shown by F6 formulation against *E. coli* (Fig. 9A), *S. aureus* (Fig. 9B), *B. subtilis* (Fig. 9C), *X. campestris* (Fig. 9D) and *A. niger* (Fig. 9E) were  $11.01 \pm 0.01$  mm,  $8.10 \pm 0.11$  mm,  $11.03 \pm 0.06$  mm,  $12.00 \pm 0.08$  mm, and  $11.15 \pm 0.03$  mm, respectively. In comparison, the standard commercial product exhibited zones of inhibition of  $12.18 \pm 0.18$  mm,  $16.06 \pm 0.05$  mm,  $14.08 \pm 0.24$  mm,  $15.11 \pm 0.24$  mm, and  $13.19 \pm 0.27$  mm, respectively. One-way ANOVA revealed significant differences in zones of inhibition between F6 and the standard

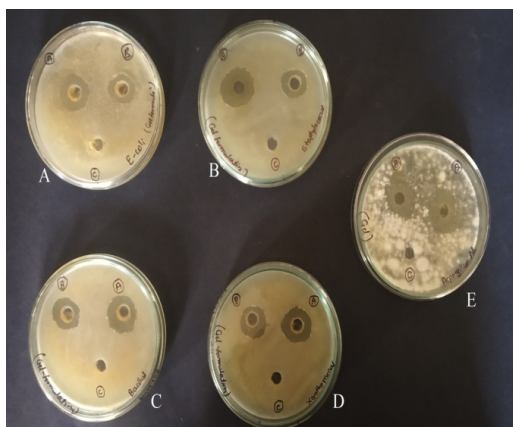


**Figure 9.** Antibacterial and antifungal activity of AgNPs-loaded gel (F6) against (A) *E. coli* (B) *S. aureus*, (C) *B. subtilis*, (D) *X. campestris* and (E) *A. niger*.

commercial product for all tested microbes ( $P < 0.05$ ). F6 showed lower inhibition compared to commercial product, suggesting slightly weaker antibacterial efficacy. Further optimization may enhance F6's performance.

Plant extract-mediated AgNPs often benefit from the diverse bioactive compounds present in the extracts, which can contribute to their antimicrobial activity. However, the effectiveness of these NPs can be influenced by the specific phytochemical composition, particle size, and stability of the NPs. The extract-based nature of the F6 formulation means that its antibacterial performance may not be as optimized as the standard commercial product's formulation. Commercial product typically incorporates optimized formulations and high-quality AgNPs, which can result in more consistent and potent antimicrobial activity.

While the F6 gel formulation may exhibit slightly weaker antibacterial efficacy compared to AgNPs and azithromycin, its use of plant extracts offers several notable advantages as a natural remedy. The inclusion of bioactive compounds from natural sources provides a range of potential benefits, including reduced risk of adverse effects and enhanced biocompatibility with skin. Natural remedies often possess a broad spectrum of antimicrobial activities, contributing to a holistic approach to treatment.

The F6 gel formulation could deliver active compounds in a controlled manner, potentially extending their antibacterial effects and improving skin adherence. Its natural origin might support a more sustainable and eco-friendly approach, reducing reliance on synthetic chemicals. These possibilities make the F6 gel a potentially preferable choice for topical applications, especially in settings where natural remedies are valued for their safety and environmental sustainability.

#### 4. Conclusion

In our investigation, we adopted an eco-conscious methodology, employing a green synthesis approach utilizing extracts derived from both the flowers and leaves of *B. suaveolens* to fabricate AgNPs. This methodological choice aligns with contemporary efforts towards sustainable and environmentally friendly practices in scientific research, offering distinct advantages over traditional chemical synthesis routes,

including reduced environmental impact, cost-effectiveness, and enhanced biocompatibility of the resulting nanoparticles. The successful synthesis of AgNPs was evidenced by a conspicuous alteration in the reaction mixture's color, transitioning from a colorless solution to a rich, dark brown hue, which serves as a hallmark characteristic of silver nanoparticle formation. This visual transformation was further corroborated through rigorous UV-visible spectroscopic analysis, providing empirical validation of the nanoparticle synthesis process. Subsequent in-depth characterization of the synthesized AgNPs unraveled intriguing structural nuances. XRD analysis unveiled a discernible face-centered cubic arrangement of silver crystal crystallites, exhibiting a distinct preference for development alongside the 111 planes. Such precise crystalline architecture holds profound implications for the physical and chemical properties of the nanoparticles, profoundly influencing their biological functionality and therapeutic efficacy. Notably, AgNPs derived from leaf extract demonstrated markedly enhanced activity, suggesting nuanced variations in the phytochemical composition and bioactive potential of the respective extracts. This underscores the criticality of meticulous plant source selection in green synthesis endeavors and underscores the untapped potential of *B. suaveolens* as a reservoir of bioactive compounds for nanoparticle synthesis. Furthermore, we endeavored to translate our findings into tangible biomedical applications by incorporating the synthesized AgNPs into a gel formulation and assessing its antibacterial and antifungal activities. The gel exhibited commendable efficacy against a spectrum of bacterial and fungal strains, indicative of its promise as a viable candidate for the treatment of bacterial infections or inflammation. Nevertheless, it is imperative to exercise caution and conduct further preclinical investigations, particularly animal studies, to comprehensively evaluate the safety and efficacy profile of the gel formulation *in vivo*. By leveraging the inherent bioactivity of *B. suaveolens* and harnessing the ingenuity of green synthesis methodologies, we are poised to usher in a new era of sustainable and efficacious therapeutic interventions, propelling the frontiers of nanomedicine and pharmaceutical sciences.

**Authors contributions**

Authors have contributed equally in preparing and writing the manuscript.

**Availability of data and materials**

The data that support the findings of this study are available from the corresponding author, [SJN], upon reasonable request.

**Conflict of interests**

The authors declare that they have no known competing financial interests or personal relationships that could have appeared to influence the work reported in this paper.

## References

- [1] J Annamalai and T. Nallamuthu. Green synthesis of silver nanoparticles: characterization and determination of antibacterial potency. *Appl. Nanosci.*, 6(259-265), 2016. DOI: <https://doi.org/10.1007/s13204-015-0426-6>.
- [2] A. S. Jain, P. S. Pawar, A. Sarkar, V. Junnuthula, and S. Dyawanapelly. Bionanofactories for green synthesis of silver nanoparticles: toward antimicrobial applications. *Int. J. Mol. Sci.*, 22(21):11993, 2021. DOI: <https://doi.org/10.3390/ijms222111993>.
- [3] N. Pal, M. Agarwal, and A. Ghosh. Green synthesis of silver nanoparticles using polysaccharide-based guar gum. *Mater. Today: Proc.*, 76:212–218, 2023. DOI: <https://doi.org/10.1016/j.matpr.2023.01.048>.
- [4] K. N. Thakkar, S. S. Mhatre, and R. Y. Parikh. Biological synthesis of metallic nanoparticles. *Nanomed. Nanotechnol. Biol. Med.*, 6(2): 257–262, 2010. DOI: <https://doi.org/10.1016/j.nano.2009.07.002>.
- [5] B. Sadeghi. Synthesis of silver nanoparticles using leaves aqueous extract of nasturtium officinale (no) and its antibacterial activity. *Int. J. Mol. Clin. Microbiol.*, 2:428–434, 2014.
- [6] B. Sadeghi and B. Koupae. Biogenic synthesis of silver nanoparticles using fruit aqueous extract of psidium guajava and its antibacterial activity. *J. Nanoanalysis.*, 4(2):126–133, 2017.
- [7] B. Sadeghi, F. S. Garmaroudi, M. Hashemi, H. R. Nezhad, A. Nasrollahi, S. Ardalan, and S. Ardalan. Comparison of the anti-bacterial activity on the nanosilver shapes: nanoparticles, nanorods and nanoplates. *Adv. Powder Technol.*, 23(1):22–26, 2012. DOI: <https://doi.org/10.1016/j.appt.2010.11.011>.
- [8] A. Amini Nia, K. H. Pourshamsian, and B. Sadeghi. Nano-zno impregnated on starch-a highly efficient heterogeneous bio-based catalyst for one-pot synthesis of pyranopyrimidinone and xanthene derivatives as potential. *Russ. J. Org. Chem.*, 56:1279–1288, 2020. DOI: <https://doi.org/10.1134/S1070428020070234>.
- [9] I. X. Yin, J. Zhang, I. S. Zhao, M. L. Mei, Q. Li, and C. H. Chu. The antibacterial mechanism of silver nanoparticles and its application in dentistry. *Int. J. Nanomedicine.*, 15:2555–2562, 2020. DOI: <https://doi.org/10.2147/IJN.S246764>.
- [10] Y. Li, P. Leung, L. Yao, Q. Song, and E. Newton. Antimicrobial effect of surgical masks coated with nanoparticles. *J. Hosp. Infect.*, 62(1):58–63, 2006. DOI: <https://doi.org/10.1016/j.jhin.2005.04.015>.
- [11] A. Martinez-Higuera, C. Rodriguez-Beas, J. M. A. Villalobos-Noriega, A. Arizmendi-Grijalva, C. Ochoa-Sanchez, E. Larios-Rodriguez, J. M. Martinez-Soto, E. Rodriguez-Leon, C. Ibarra-Zazueta, R. Mora-Monroy, H. A. Borbon-Nunez, A. Garcia-Galaz, M. C. Candia-Plata, L. F. Lopez-Soto, and R. Iniguez-Palomares. Hydrogel with silver nanoparticles synthesized by mimosa tenuiflora for second-degree burns treatment. *Sci. Rep.*, 11(1):11312, 2021. DOI: <https://doi.org/10.1038/s41598-021-90763-w>.
- [12] S. C. Kumari, V. Dhand, and P. N. Padma. Green synthesis of metallic nanoparticles: a review. in r. praveen kumar and b. bharathiraja (ed.), *nanomaterials application in biofuels and bioenergy production system*. *Nanomaterials*, 11:259–281, 2021. DOI: <https://doi.org/10.1016/B978-0-12-822401-4.00022-2>.
- [13] P. G. Jamkhande, N. W. Ghule, A. H. Bamer, and M. G. Kalaskar. Metal nanoparticles synthesis: an overview on methods of preparation, advantages and disadvantages, and applications. *J. Drug Deliv. Sci. Technol.*, 53:101174, 2019. DOI: <https://doi.org/10.1016/j.jddst.2019.101174>.
- [14] B. Azari, A. Pourahmad, B. Sadeghi, and M. Mokhtary. Green synthesis of  $\text{SiO}_2$  from equisetum arvense plant for synthesis of  $\text{SiO}_2/\text{ZIF-8}$  mof nanocomposite as photocatalyst. *J. Coord. Chem.*, 76(2): 219–231, 2023. DOI: <https://doi.org/10.1080/00958972.2023.2166408>.
- [15] K. McNamara, S. A. Tofail, N. D. Thorat, J. Bauer, and J. J. Mulvihill. Biomedical applications of nanoalloys. *Nanoalloys.*, 15:381–432, 2020. DOI: <https://doi.org/10.1016/B978-0-12-819847-6.00016-4>.
- [16] S. Dessai, M. Ayyanar, S. Amalraj, P. Khanal, S. Vijayakumar, N. Gurav, N. Rarokar, M. Kalaskar, S. Nadaf, and S. Gurav. Bioflavonoid mediated synthesis of  $\text{TiO}_2$  nanoparticles: characterization and their biomedical applications. *Mater. Lett.*, 311:131639, 2022. DOI: <https://doi.org/10.1016/j.matlet.2021.131639>.
- [17] B. Sadeghi, M. Mohammadzadeh, and B. Babakhani. Green synthesis of gold nanoparticles using stevia rebaudiana leaf extracts: characterization and their stability. *J. Photochem. Photobiol. B: Biol.*, 148:101–106, 2015. DOI: <https://doi.org/10.1016/j.jphotobiol.2015.03.025>.
- [18] B. Sadeghi. Green synthesis of silver nanoparticles using seed aqueous extract of olea europaea. *Int. J. Nano Dimens.*, 5(6):575–581, 2024. DOI: <https://doi.org/10.7508/ijnd.2014.06.010>.
- [19] J. Jahani, M. Ghane, and B. Sadeghi. Biosynthesis of silver nanoparticles using native acetobacter and pediococcus strains. *Int. J. Mol. Clin. Microbiol.*, 11(1):1479–1488, 2021.
- [20] M. Kaur, A. Gautam, P. Guleria, K. Singh, and V. Kumar. Green synthesis of metal nanoparticles and their environmental applications. *Curr. Opin. Environ. Sci. Health.*, 29:100390, 2022. DOI: <https://doi.org/10.1016/j.coesh.2022.100390>.
- [21] S. Prabhu and E. K. Poullose. Silver nanoparticles: mechanism of antimicrobial action, synthesis, medical applications, and toxicity effects. *Int. Nano Lett.*, 2:1–10, 2012. DOI: <https://doi.org/10.1186/2228-5326-2-32>.
- [22] D. Philip, C. Unni, S. A. Aromal, and V. Vidhu. Murraya koenigii leaf-assisted rapid green synthesis of silver and gold nanoparticles. *Spectrochim. Acta A: Mol. Biomol. Spectrosc.*, 78(2):899–904, 2011. DOI: <https://doi.org/10.1016/j.saa.2010.12.060>.
- [23] P. G. Jamkhande, N. W. Ghule, A. H. Bamer, and M. G. Kalaskar. Metal nanoparticles synthesis: an overview on methods of preparation, advantages and disadvantages, and applications. *J. Drug Deliv. Sci. Technol.*, 53:101174, 2019. DOI: <https://doi.org/10.1016/j.jddst.2019.101174>.
- [24] N. Pantidos and L. E. Horsfall. Biological synthesis of metallic nanoparticles by bacteria, fungi and plants. *J. Nanomed. Nanotechnol.*, 5(5):1, 2014. DOI: <https://doi.org/10.4172/2157-7439.1000233>.
- [25] D. Philip. Mangifera indica leaf-assisted biosynthesis of well-dispersed silver nanoparticles. *Spectrochim. Acta A: Mol. Biomol. Spectrosc.*, 78(1):327–331, 2011. DOI: <https://doi.org/10.1016/j.saa.2010.10.015>.

- [26] K. Ahmad, H. M. Asif, T. Afzal, M. A. Khan, M. Younus, U. Khurshid, M. Safdar, S. Saifulah, B. Ahmad, A. Sufyan, S. A. Ansari, H. M. Alkahtani, and I. A. Ansari. Green synthesis and characterization of silver nanoparticles through the piper cubeba ethanolic extract and their enzyme inhibitory activities. *Front. Chem.*, 11:1065986, 2023. DOI: <https://doi.org/10.3389/fchem.2023.1065986>.
- [27] R. Yadav, H. Saini, D. Kumar, S. Pasi, and V. Agrawal. Bioengineering of piper longum l. extract mediated silver nanoparticles and their potential biomedical applications. *Mater. Sci. Eng. C.*, 104:109984, 2019. DOI: <https://doi.org/10.1016/j.msec.2019.109984>.
- [28] S. Singla, A. Jana, R. Thakur, C. Kumari, S. Goyal, and J. Pradhan. Green synthesis of silver nanoparticles using oxalis griffithii extract and assessing their antimicrobial activity. *OpenNano*, 7:100047, 2022. DOI: <https://doi.org/10.1016/j.onano.2022.100047>.
- [29] A. W. Alshameri, M. Owais, I. Altaf, and S. Farheen. Rumex nervosus mediated green synthesis of silver nanoparticles and evaluation of its in vitro antibacterial, and cytotoxic activity. *OpenNano*, 8:100084, 2022. DOI: <https://doi.org/10.1016/j.onano.2022.100084>.
- [30] J. Prapaipittayakhun, S. Boonyuen, A. L. T. Zheng, K. Apinyaupatham, and P. Arpornmaeklong. Biologic effects of biosynthesized oroxyllum indicum/silver nanoparticles on human periodontal ligament stem cells. *OpenNano*, 9:100117, 2023. DOI: <https://doi.org/10.1016/j.onano.2022.100117>.
- [31] B. Sadeghi, A. Rostami, and S. S. Momeni. Facile green synthesis of silver nanoparticles using seed aqueous extract of pistacia atlantica and its antibacterial activity. *Spectrochim. Acta A: Mol. Biomol. Spectrosc.*, 134:326–332, 2015. DOI: <https://doi.org/10.1016/j.saa.2014.05.078>.
- [32] B. Sadeghi and B. Koupaei. Biological synthesis of silver nanoparticles using the aqueous extract of psidium guajava (pg) and its antibacterial activity. *J. Med. Biol. Sci.*, 12(2):21–33, 2022.
- [33] S. Pundir, M. K. Shukla, A. Singh, R. Chauhan, U. R. Lal, A. Ali, and D. Kumar. A comprehensive review on angel's trumpet (brugmansia suaveolens). *S. Afr. J. Bot.*, 151:266–274, 2022. DOI: <https://doi.org/10.1016/j.sajb.2022.02.023>.
- [34] S. Kumar, A. Gupta, R. V. Saini, A. Kumar, K. L. Dhar, and N. Mahindroo. Immunomodulation-mediated anticancer activity of a novel compound from brugmansia suaveolens leaves. *Bioorg. Med. Chem.*, 28(12):115552, 2020. DOI: <https://doi.org/10.1016/j.bmc.2020.115552>.
- [35] V. L. Petricevich, D. O. Salinas-Sánchez, D. Avilés-Montes, C. Sotelo-Leyva, and R. Abarca-Vargas. Chemical compounds, pharmacological and toxicological activity of brugmansia suaveolens: a review. *Plants (Basel)*, 9(9):1161, 2020. DOI: <https://doi.org/10.3390/plants9091161>.
- [36] A. G. Parker, G. G. Peraza, J. Sena, E. S. Silva, M. C. F. Soares, M. R. C. Vaz, E. B. Furlong, and A. L. Muccillo-Baisch. Antinociceptive effects of the aqueous extract of brugmansia suaveolens flowers in mice. *Biol. Res. Nurs.*, 8(3):234–239, 2007. DOI: <https://doi.org/10.1177/1099800406293984>.
- [37] A. L. Muccillo-Baisch, A. G. Parker, G. P. Cardoso, M. R. Cezar-Vaz, and M. C. Flores Soares. Evaluation of the analgesic effect of aqueous extract of brugmansia suaveolens flower in mice: possible mechanism involved. *Biol. Res. Nurs.*, 11(4):345–350, 2010. DOI: <https://doi.org/10.1177/1099800409354123>.
- [38] G. R. Brito, M. B. de Lima, G. C. Maciel, and M. S. Santos. Antibacterial activity of crude aqueous solution of brugmansia suaveolens flowers. *Res. Soc. Dev.*, 12(2):e7112238140, 2023. DOI: <https://doi.org/10.33448/rsd-v12i2.38140>.
- [39] J. Jain, S. Arora, J. M. Rajwade, P. Omay, S. Khandelwal, and K. M. Paknikar. Silver nanoparticles in therapeutics: development of an antimicrobial gel formulation for topical use. *Mol. Pharm.*, 6(5):1388–1401, 2009. DOI: <https://doi.org/10.1021/mp900056g>.
- [40] S. Khogta, J. Patel, K. Barve, and V. Londhe. Herbal nano-formulations for topical delivery. *J. Herb. Med.*, 20:100300, 2020. DOI: <https://doi.org/10.1016/j.hermed.2019.100300>.
- [41] G. Franceschinis, M. Beverina, M. Corleto, A. M. Sosa, C. Lillo, L. A. Casarà, S. V. Alonso, P. Maffia, J. Montanari, M. E. Tuttolomondo, and M. N. Calieni. Green-synthesized silver nanoparticles using aloe maculata extract as antibacterial agent for potential topical application. *OpenNano*, 12:100148, 2023. DOI: <https://doi.org/10.1016/j.onano.2023.100148>.
- [42] S. J. Nadaf, S. G. Killedar, V. M. Kumbar, D. A. Bhagwat, and S. S. Gurav. Pazopanib-laden lipid based nanovesicular delivery with augmented oral bioavailability and therapeutic efficacy against non-small cell lung cancer. *Int. J. Pharm.*, 628:122287, 2022. DOI: <https://doi.org/10.1016/j.ijpharm.2022.122287>.
- [43] S. Devanesan and M. S. AlSalhi. Green synthesis of silver nanoparticles using the flower extract of abelmoschus esculentus for cytotoxicity and antimicrobial studies. *Int. J. Nanomedicine*, pages 3343–3356, 2021. DOI: <https://doi.org/10.2147/IJN.S307676>.
- [44] C. Dias, M. Ayyanar, S. Amalraj, P. Khanal, V. Subramaniyan, S. Das, P. Gandhale, V. Biswa, R. Ali, N. Gurav, S. Nadaf, N. Rarokar, and S. Gurav. Biogenic synthesis of zinc oxide nanoparticles using mushroom fungus cordyceps militaris: characterization and mechanistic insights of therapeutic investigation. *J. Drug Deliv. Sci. Technol.*, 73:103444, 2022. DOI: <https://doi.org/10.1016/j.jddst.2022.103444>.
- [45] M. Balouiri, M. Sadiki, and S. K. Ibnsouda. Methods for in vitro evaluating antimicrobial activity: A review. *J. Pharm. Anal.*, 6(2):71–79, 2016. DOI: <https://doi.org/10.1016/j.jpha.2015.11.005>.
- [46] H. Jahangirian, M. J. Haron, M. H. Shah, Y. Abdollahi, M. Rezayi, and N. Vafaei. Well diffusion method for evaluation of antibacterial activity of copper phenyl fatty hydroxamate synthesized from canola and palm kernel oils. *Dig. J. Nanomater. Biostructures*, 8(3):1263–1270, 2013.
- [47] I. Moualek, G. I. Aiche, N. M. Guechaoui, S. Lahcene, and K. Houali. Antioxidant and anti-inflammatory activities of arbutus unedo aqueous extract. *Asian Pac. J. Trop. Biomed.*, 6(11):937–944, 2016. DOI: <https://doi.org/10.1016/j.apjtb.2016.09.002>.
- [48] M. G. B. Dantas, S. A. G. B. Reis, C. M. D. Damasceno, L. A. Rolim, P. J. Rolim-Neto, F. O. Carvalho, and J. R. G. da Silva Almeida. Development and evaluation of stability of a gel formulation containing the monoterpene borneol. *Sci. World J.*, pages 1–7, 2016. DOI: <https://doi.org/10.1155/2016/7394685>.
- [49] S. M. Morsy, I. S. Elbasyoni, A. M. Abdallah, and P. S. Baenziger. Imposing water deficit on modern and wild wheat collections to identify drought-resilient genotypes. *J. Agron. Crop Sci.*, 208(4):427–440, 2022. DOI: <https://doi.org/10.1111/jac.124>.
- [50] K. P. M. Haneefa, H. K. Shahima, R. Saraswathi, G. P. Mohanta, and C. Nayar. Formulation and evaluation of herbal gel of pothos scandens linn. *Asian Pac. J. Trop. Med.*, 3(12):988–992, 2010. DOI: [https://doi.org/10.1016/S1995-7645\(11\)60015-1](https://doi.org/10.1016/S1995-7645(11)60015-1).
- [51] L. N. R. Katakam and N. K. Katari. Development of in-vitro release testing method for permethrin cream formulation using franz vertical diffusion cell apparatus by hplc. *Talanta Open*, 4:100056, 2021. DOI: <https://doi.org/10.1016/j.talo.2021.100056>.
- [52] M. C. Dias, D. C. Pinto, and A. M. Silva. Plant flavonoids: chemical characteristics and biological activity. *Molecules*, 26(17):5377, 2021. DOI: <https://doi.org/10.3390/molecules26175377>.

- [53] U. Ejaz, M. Afzal, M. Mazhar, M. Riaz, N. Ahmed, W. Y. Rizg, A. A. Alahmadi, M. Y. Badr, R. Y. Mushtaq, and C. Y. Yean. Characterization, synthesis, and biological activities of silver nanoparticles produced via green synthesis method using thymus vulgaris aqueous extract. *Int. J. Nanomed.*, 19:453–469, 2024. DOI: <https://doi.org/10.2147/IJN.S446017>.
- [54] N. S. Alharbi, N. S. Alsubhi, and A. I. Felimban. Green synthesis of silver nanoparticles using medicinal plants: characterization and application. *J. Radiat. Res. Appl. Sci.*, 15(3):109–124, 2022. DOI: <https://doi.org/10.1016/j.jrras.2022.06.012>.
- [55] C. Vanlalveni, S. Lallianrawna, A. Biswas, M. Selvaraj, B. Changmai, and S. L. Rokhum. Green synthesis of silver nanoparticles using plant extracts and their antimicrobial activities: a review of recent literature. *RSC Adv.*, 11(5):2804–2837, 2021. DOI: <https://doi.org/10.1039/d0ra09941d>.
- [56] A. Pan, Z. Yang, H. Zheng, F. Liu, Y. Zhu, X. Su, and Z. Ding. Changeable position of spr peak of ag nanoparticles embedded in mesoporous sio<sub>2</sub> glass by annealing treatment. *Appl. Surf. Sci.*, 205(1-4):323–328, 2003. DOI: [https://doi.org/10.1016/S0169-4332\(02\)01122-4](https://doi.org/10.1016/S0169-4332(02)01122-4).
- [57] A. Amirjani, F. Firouzi, and D. F. Haghsheenas. Predicting the size of silver nanoparticles from their optical properties. *Plasmonics.*, 15:1077–1082, 2020. DOI: <https://doi.org/10.1007/s11468-020-01121-x>.
- [58] N. Duran, P. D. Marcato, G. I. De Souza, O. L. Alves, and E. Esposito. Antibacterial effect of silver nanoparticles produced by fungal process on textile fabrics and their effluent treatment. *J. Biomed. Nanotechnol.*, 3(2):203–208, 2007. DOI: <https://doi.org/10.1166/jbn.2007.022>.
- [59] D. G. Nkosinathi, B. K. Albertus, S. S. Jabulani, S. M. Siboniso, and R. V. Pullabhotla. Biosynthesis, characterization, and application of iron nanoparticles: in dye removal and as antimicrobial agent. *Water Air Soil Pollut.*, 231:1–10, 2020. DOI: <https://doi.org/10.1007/s11270-020-04498-x>.
- [60] A. K. Singh. A review on plant extract-based route for synthesis of cobalt nanoparticles: photocatalytic, electrochemical sensing and antibacterial applications. *Curr. Res. Green Sustain. Chem.*, 5:100270, 2022. DOI: <https://doi.org/10.1016/j.crgsc.2022.100270>.
- [61] S. K. Srikar, D. D. Giri, D. B. Pal, P. K. Mishra, and S. N. Upadhyay. Green synthesis of silver nanoparticles: a review. *Green Sustain. Chem.*, 6(1):34–44, 2016. DOI: <https://doi.org/10.4236/GSC.2016.61004>.
- [62] S. Kumar, I. B. Basumatary, H. P. Sudhani, V. K. Bajpai, L. Chen, S. Shukla, and A. Mukherjee. Plant extract mediated silver nanoparticles and their applications as antimicrobials and in sustainable food packaging: a state-of-the-art review. *Trends Food Sci. Technol.*, 112:651–666, 2021. DOI: <https://doi.org/10.1016/J.TIFS.2021.04.031>.
- [63] M. Z. Shah, Z. H. Guan, A. Ud Din, A. Ali, A. Ur Rehman, K. Jan, S. Faisal, S. Saud, M. Adnan, F. Wahid, S. Alamri, M. H. Siddiqui, S. Ali, W. Nasim, H. M. Hammad, and S. Fahad. Synthesis of silver nanoparticles using plantago lanceolata extract and assessing their antibacterial and antioxidant activities. *Sci. Rep.*, 11(1):20754, 2021. DOI: <https://doi.org/10.1038/s41598-021-00296-5>.
- [64] S. B. Parit, V. C. Karade, R. B. Patil, N. V. Pawar, R. P. Dhavale, M. Tawre, K. Pardesi, U. U. Jadhav, V. V. Dawkar, R. S. Tanpure, J. H. Kim, J. P. Jadhav, and A. D. Chougale. Bioinspired synthesis of multifunctional silver nanoparticles for enhanced antimicrobial and catalytic applications with tailored spr properties. *Mater. Today Chem.*, 17:100285, 2020. DOI: <https://doi.org/10.1016/j.mtchem.2020.100285>.
- [65] H. Padalia, P. Moteriya, and S. Chanda. Green synthesis of silver nanoparticles from marigold flower and its synergistic antimicrobial potential. *Arab. J. Chem.*, 8(5):732–741, 2015. DOI: <https://doi.org/10.1016/j.arabjc.2014.11.015>.
- [66] M. Gomathi, P. Rajkumar, A. Prakasam, and K. Ravichandran. Green synthesis of silver nanoparticles using datura stramonium leaf extract and assessment of their antibacterial activity. *Resource-Efficient Technol.*, 3(3):280–284, 2017. DOI: <https://doi.org/10.1016/j.reffit.2016.12.005>.
- [67] E. Urnukhsaikhan, B. E. Bold, A. Gunbileg, N. Sukhbaatar, and T. Mishig-Ochir. Antibacterial activity and characteristics of silver nanoparticles biosynthesized from carduus crispus. *Sci. Rep.*, 11(1):21047, 2021. DOI: <https://doi.org/10.1038/s41598-021-00520-2>.
- [68] H. Agarwal, A. Nakara, and V. K. Shanmugam. Anti-inflammatory mechanism of various metal and metal oxide nanoparticles synthesized using plant extracts: a review. *Biomed. Pharmacother.*, 109:2561–2572, 2019. DOI: <https://doi.org/10.1016/j.biopha.2018.11.116>.
- [69] M. Schafer and S. Werner. Oxidative stress in normal and impaired wound repair. *Pharmacol. Res.*, 58(2):165–171, 2008. DOI: <https://doi.org/10.1016/j.phrs.2008.06.004>.
- [70] H. Zhao, J. Huang, Y. Li, X. Lv, H. Zhou, H. Wang, Y. Xu, C. Wang, J. Wang, and Z. Liu. Ros-scavenging hydrogel to promote healing of bacteria infected diabetic wounds. *Biomaterials.*, 258:120286, 2020. DOI: <https://doi.org/10.1016/j.biomaterials.2020.120286>.